1-1-2001

Protoporphyrin IX distribution in rat brain following the administration of 5-aminolevulinic acid and its hexylester

Scott Alan Friesen
University of Nevada, Las Vegas

INFORMATION TO USERS

This manuscript has been reproduced from the microfilm master. UMI films the text directly from the original or copy submitted. Thus, some thesis and dissertation copies are in typewriter face, while others may be from any type of computer printer.

The quality of this reproduction is dependent upon the quality of the copy submitted. Broken or indistinct print, colored or poor quality illustrations and photographs, print bleedthrough, substandard margins, and improper alignment can adversely affect reproduction.

In the unlikely event that the author did not send UMI a complete manuscript and there are missing pages, these will be noted. Also, if unauthorized copyright material had to be removed, a note will indicate the deletion.

Oversize materials (e.g., maps, drawings, charts) are reproduced by sectioning the original, beginning at the upper left-hand corner and continuing from left to right in equal sections with small overlaps.

ProQuest Information and Learning
300 North Zeeb Road, Ann Arbor, MI 48106-1346 USA
800-521-0600

PROTOPORPHYRIN IX DISTRIBUTION IN RAT BRAIN FOLLOWING THE ADMINISTRATION OF 5-AMINOLEVULINIC ACID AND ITS HEXYLESTER

by

Scott Alan Friesen

Bachelor of Arts, Biology
Bethel College, Kansas
1998

A thesis submitted in partial fulfillment
of the requirements for the degree of

Master of Science Degree
Department of Health Physics
College of Health Sciences

Graduate College
University of Nevada, Las Vegas
August 2002

ProQuest Information and Learning Company
300 North Zeeb Road
P.O. Box 1346
Ann Arbor, MI 48106-1346

UNLV

Thesis Approval
The Graduate College
University of Nevada, Las Vegas

July 22, 2002

The Thesis prepared by

Scott A. Friesen

Entitled

Protoporphyrin IX Distribution in Rat Brain Following the Administration of 5-Aminolevulinic Acid and its Hexylester

is approved in partial fulfillment of the requirements for the degree of

Master of Science

Examination Committee Chair

Dean of the Graduate College

Examination Committee Member

Examination Committee Member

Graduate College Faculty Representative

ABSTRACT

Protoporphyrin IX Distribution in Rat Brain Following the Administration of 5-Aminolevulinic Acid and its Hexylester

by

Scott A. Friesen

Dr. Steen J. Madsen, Examination Committee Chair
Assistant Professor of Health Physics
University of Nevada, Las Vegas

Rowett nude rats were injected intra-cranially with varying concentrations of 5-aminolevulinic acid (10, 20, 99, 199, 398 mM) and its hexylester (6.6, 13, 66, 132, 265 mM). Toxicity effects of these compounds were examined based on animal behavior and respiratory distress. It was determined that the maximum tolerable dose for intra-cranial injection is 99 mM 5-Aminolevulinic acid and 66 mM h-ALA.

Human glioma spheroids were grown *in vitro*. After incubation, spheroids were sized (250-350 μm) and injected into the rat brain (10 spheroids per injection). Following the induction and development of glioblastoma multiforme tumors *in vivo*, Rowett nude rats were injected with the maximum tolerable ALA or h-ALA dose. Animals were sacrificed four hours post-injection and intact brains were removed. Fluorescence microscopy was performed to quantify PpIX production. Results indicate that PpIX production in tumor tissue is greater following 5-aminolevulinic acid administration than h-ALA. However, the tumor-to-normal tissue uptake ratio is superior following injection of h-ALA (7.6±2.0:1) compared to 5-aminolevulinic acid (2.4±1.1:1).

TABLE OF CONTENTS

LIST OF FIGURES

LIST OF TABLES

ACKNOWLEDGMENTS

Funding for this project was provided by the University of Nevada, Las Vegas Graduate College and PhotoCure. The development of this project was made possible by the cooperation of the Pathology and Tumor Biology Departments, Norwegian Radium Hospital and the Department of Neurosurgery, Norwegian National Hospital. Several individuals contributed to the development of this project and merit my gratitude for their expertise and support.

I am especially grateful to my advisor, Dr. Steen J. Madsen, for his continued guidance throughout the development of this thesis as well as many of my other academic endeavors. I wish to thank Dr. William H. Johnson for his enthusiasm and encouragement during my journey through the Health Physics program. My appreciation extends to the other members of my Thesis Examination Committee, Dr. Henry Hirschberg and Dr. Stephen W. Carper, for their support in this project.

Many thanks to Dr. Qian Peng for his advice and confidence, and for providing me with opportunities extending beyond this project. For their knowledge in the laboratory and for providing technical assistance, I thank Dr. Geir Olav Hjortland, Dr. Olav Engebraaten, Solveig Garmon-Vik, and Fabio Apricena. These individuals made my research in Norway a valuable and memorable experience.

Additionally, I wish to recognize several people for their personal and moral support throughout this project as well as my life. I thank my parents, Alan and Sharon, for

instilling in me the determination and confidence that has allowed me to pursue my dreams. I thank my brother, Shaun, for his friendship. To Kim, thank you for joining me in Norway, and for providing your significant support throughout this venture.

I am indebted to the individuals mentioned above who contributed in so many ways. I extend my deepest appreciation to all of you.

CHAPTER 1

INTRODUCTION

1.1 Overview of Photodynamic Therapy

Photodynamic Therapy (PDT) involves the administration of a tumor-specific photosensitizing agent that, upon subsequent activation by a particular wavelength of light, results in tumor tissue necrosis. Although PDT is a relatively new cancer treatment modality, the use of photosensitizing agents in combination with light irradiation has been used in both diagnostic and therapeutic medicine for the past 3 decades (Dougherty *et al* 1998). Current uses of PDT include treatment of skin cancer and dermatological diseases, esophageal cancer, bladder cancer, and colon cancer. The degree of efficacy associated with PDT depends on several factors including the type of photosensitizer used, concentration of the photosensitizer in tumor tissue, tissue oxygenation status, fluence of light used for irradiation, and fluence rate. For the treatment of many tumors, longer wavelengths of light are required for adequate tissue penetration. A strong attenuation occurs in tissue up to 580 nm because of absorption by hemoglobin bands, followed by an increase in light penetration over the 600-680 nm range (Moore *et al* 1997). Shorter wavelengths of light, such as green light, have been utilized where relatively deep tissue penetration must be avoided (e.g. in bladder cancer and colorectal tumors).

1.1.1 Photochemistry

Following light irradiation, the absorption of a photon causes the activation of the photosensitizer to an excited triplet state (Oleinick and Evans 1999). The triplet may undergo one of two types of photochemical reactions. The type I reaction involves electron transfer between the photosensitizer triplet and surrounding molecules. This redox reaction yields a substrate radical that participates in radical chain reactions. These radicals interact primarily with oxygen and generate reactive oxygen intermediates such as H_2O_2, $\bullet O_2^-$, and •OH.

The type II mechanism, or singlet oxygen hypothesis, has been widely accepted as the primary photochemical mode of PDT-induced damage (Weishaupt *et al* 1976, Moan *et al* 1992, Henderson and Dougherty 1992, Ochsner 1997, Hasan and Parrish 1997). Molecular oxygen in the singlet state ($^1O_2$) is produced when a photosensitizer triplet interacts with ambient molecular oxygen. Although $^1O_2$ is a nonradical, it is highly reactive and can damage cellular structures. Since $^1O_2$ has a maximum diffusion range of 20 nm (Moan and Berg 1991) and a lifetime less than 0.5 μs (Patterson *et al* 1990), and human cells range from 10 μm to 100 μm in diameter, the location at which $^1O_2$ is produced determines which structures in the cell are damaged.

Photosensitizers have also been reported to exist in high concentrations in tumor vasculature (Moan and Berg 1992, Henderson and Dougherty 1992, Hasan and Parrish 1997). Therefore, singlet molecular oxygen generation can also occur outside of tumor cells in the epithelial cells of vascular tissue. In this case, cell death occurs indirectly by eliminating the tumor's blood supply (blood flow stasis, vasculature collapse, or leakage).

1.1.2 Photobiology

The specific mechanism of cell death following light excitation of photosensitizers has been the focus of recent PDT-related research. Photodamage may cause cell death by either necrosis or apoptosis - the mode of cell death being dependent on a number of factors including cell type, photosensitizer type and concentration, subcellular localization of the sensitizer (Kessel *et al* 1997, Kessel and Luo 1998, Kessel *et al* 1998) and light dose (Luo and Kessel 1997, He and Oleinick 1995). Necrosis involves cell membrane fragmentation followed by the release of cellular contents into the surrounding medium. This process usually elicits an inflammatory response resulting from the interaction of lysosomal enzymes with adjoining cells. Apoptosis (programmed cell death) is initiated by cellular signals, resulting in organized DNA and cellular fragmentation followed by the encapsulation of these fragments into apoptotic bodies by surrounding cells (Kerr *et al* 1972, Williams 1991, Vaux and Strassner 1996). Originally, it was believed that PDT-induced cell death proceeded by cellular necrosis (Moan and Berg 1992, Henderson and Dougherty 1992). However, an apoptotic mechanism has been implicated in PDT-related photodamage (Agarwal *et al* 1991, He *et al* 1994, Zaidi *et al* 1993, Luo *et al* 1996). Apoptosis may be induced by diverse stimuli such as radiation, chemotherapy (Wyllie 1985, Fisher 1994), and PDT (Noodt *et al* 1996). Several studies have supported the apoptotic mode of cell death following PDT *in vitro* (Agarwal *et al* 1991, He *et al* 1994) and *in vivo* (Webber *et al* 1996, Zaidi *et al* 1993). It has been demonstrated that the apoptotic process is triggered by a mitochondrial component called cytochrome *c* (Liu *et al* 1996, Yang *et al* 1997, Kluck *et al* 1997). Thus, therapies resulting in mitochondrial damage, and subsequent release of cytochrome c, are likely to

induce apoptosis. As previously mentioned, the site of cellular damage is dependent on photosensitizer type. Some sensitizers have been shown to elicit a rapid apoptotic response whereas others induce membrane and lysosme damage which lead to necrosis (Kessel and Luo 1998). The apoptotic mode of cell death may be preferred to tumor cell necrosis in PDT (especially in the brain) since the former does not result in an aggressive inflammatory response or the release of intra-cellular contents into the extra-cellular environment (Webber *et al* 1996).

1.1.3 Photosensitizers

Photosensitizers may be administered locally or systemically (intravenously, intraperitoneally, or orally) depending on the treatment. Traditionally, porphyrin-based photosensitizers such as Hematoporphyrin Derivative (HpD) and its purified version, Photofrin® (QLT PhotoTherapeutics Inc., Vancouver, B.C., Canada) have been used almost exclusively in PDT. While HpD and Photofrin are effective clinical PDT drugs, several limitations exist. Associated with these compounds is a relatively poor light absorption at long wavelengths ($\geq$ 600 nm), chemical complexity, and prolonged cutaneous photosensitization (4-6 weeks). Such a lengthy skin sensitization period adversely affects patients' quality of life. Due to the drawbacks of traditional porphyrins, other photosensitizers are currently being evaluated for use in PDT. Endogenously synthesized sensitizers such as 5-aminolevulinic acid (ALA) and its esters have been studied extensively and utilized effectively in many cancer treatments, primarily skin lesions (Peng *et al* 1997, Peng *et al* 2001). Other newly developed photosensitizers include tin etiopurpurin (SnET2), benzoporphyrin derivative-monoacid ring A (BPD-MA), lutetium texaphyrin (Lu-tex), and tetra(m-hydroxyphenyl)chlorin (mTHPC).

All human cells except mature red blood cells are capable of synthesizing heme. In the first step of the heme biosynthetic pathway, ALA is formed from succinyl CoA and glycine. The potent photosensitizer, protoporphyrin IX (PpIX), is produced from protoporphyrinogen IX in the second-to-last step of this pathway. In the last step of the pathway iron is incorporated into PpIX under the enzymatic action of ferrocheletase in the mitochondria. Due to the limited capacity of ferrocheletase, the exogenous administration of ALA results in an intra-cellular accumulation of PpIX. Compound selectivity is achieved through an enzyme activity difference between tumor cells and normal cells. Ferrocheletase activity and its capacity for incorporating iron into PpIX is limited in tumor cells and, therefore, results in a greater accumulation of PpIX. Further, the intermediary enzyme porphobilinogen deaminase exhibits increased activity in tumor cells leading to a faster PpIX production. With quicker PpIX production in tumor cells and the subsequent inability to efficiently convert PpIX to heme, exogenous ALA administration provides superior tumor selectivity to its HpD and Photofrin counterparts (Lilge and Wilson 1998). Maximal PpIX production occurs roughly four hours after administration in most cells (Olivo *et al* 1998, Xiao *et al* 1998) and it is therefore most desirable to treat at this time. Other major advantages of ALA are a dramatically shorter cutaneous photosensitization period of 24-48 hours (permitting repeat or fractionated treatments) and easy administration (oral or topical).

It should be noted that ALA is a hydrophilic compound. While ALA demonstrates tumor selectivity with regards to intra-cellular processes, its hydrophilic chemical nature limits transport across intact (lipophilic) cellular membranes. The modification of ALA to a lipophilic chemical state is possible by esterification (Kloek and van Henegouwen

1996, Kloek *et al* 1998). ALA ester lipophilicity is reflected by the octanol water partition coefficient as outlined in Table 1. ALA and the methylester are soluble in water but less so in octanol. Conversely, the hexylester (h-ALA) and benzylester are more soluble in octanol and less soluble in water. The finding that comparable amounts of PpIX are produced following the administration of ALA and lower concentrations of ALA ester, reflects the superior ability of esters to penetrate cell membranes (Uehlinger *et al* 2000). Increased ALA ester-induced PDT efficacy has also been reported in experiments involving human glioma spheroids (Hirschberg *et al* 2002). PpIX production is not only dependent on the photosensitizer concentration, but on the ability of cells to cleave the ester component (enzymatic action of esterases) and release ALA into the heme pathway (Kloek *et al* 1998).

Table 1 Octanol Water Partition Coefficients of ALA and Esters

Photosensitizing Compound	Molar Weight ($g\ mol^{-1}$)	log P[a] Octanol Water
5-Aminolevulinate HCl (ALA)	167	-1.4
Methyl 5-Aminolevulinate HCl	181	-0.8
Hexyl 5-Aminolevulinate HCl	252	+2.2
Benzyl 5-Aminolevulinate HCl	257	+2.4

[a] log P is the logarithm of a compound's partition coefficient between octanol and water. It is a physicochemical parameter that correlates with absorption of small molecules into physiological membranes.

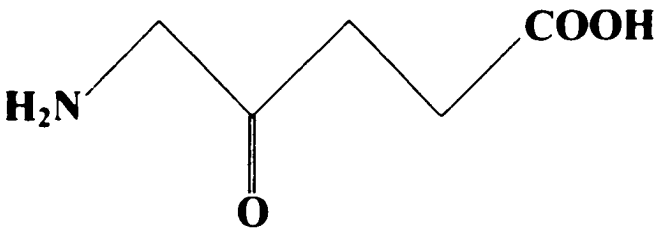

Figure 1. Chemical Structure of 5-ALA

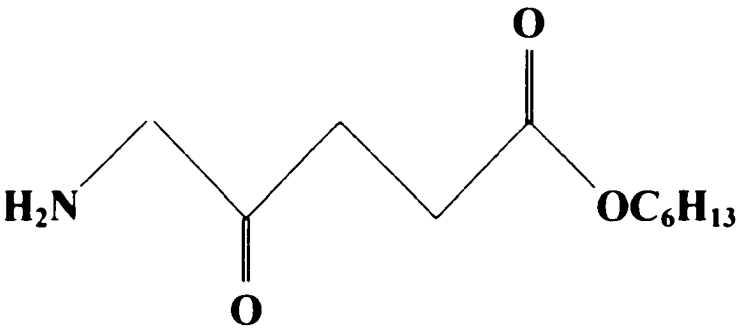

Figure 2. Chemical Structure of h-ALA

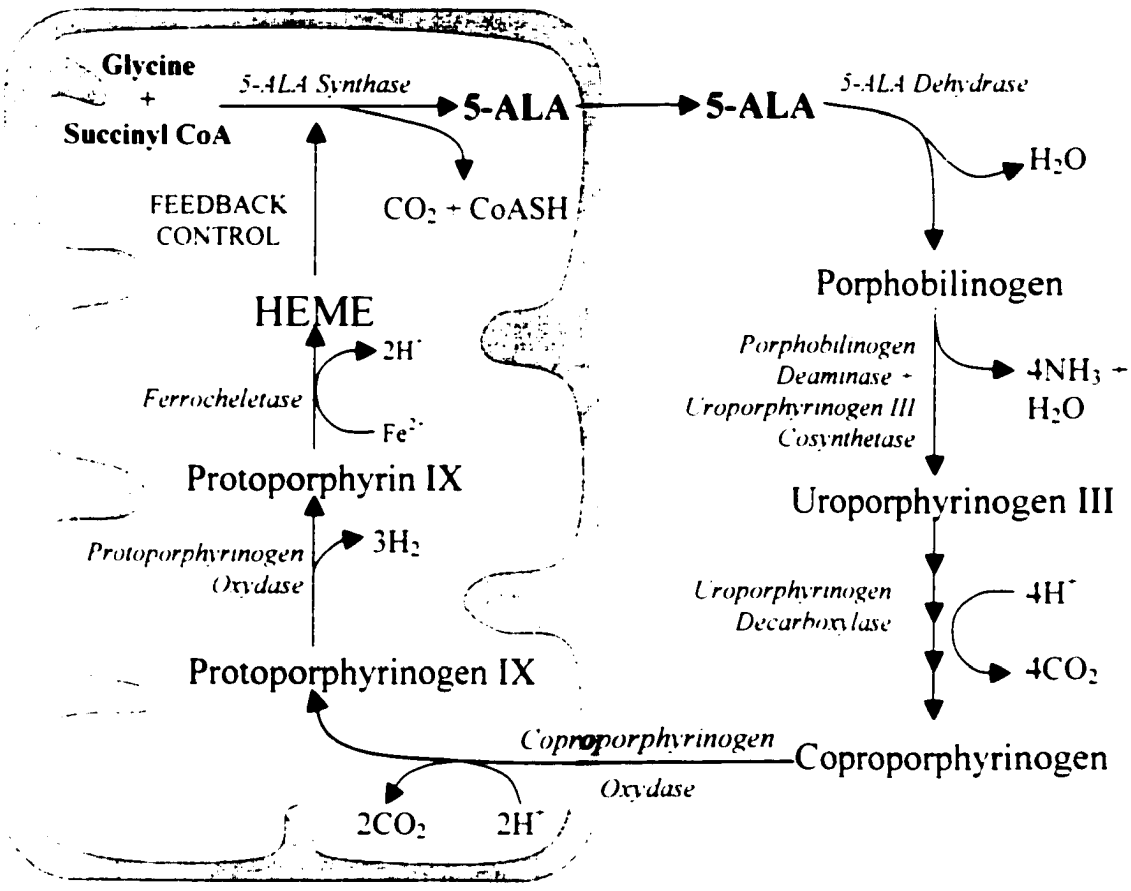

Figure 3. Heme Biosynthesis Pathway

1.1.4 Pharmacokinetics of ALA and its esters

One of the major concerns with using ALA (and esters) as a photosensitizer relates to organ toxicity (specifically the liver). Porphyrin levels in the plasma of dogs were measured following the intravenous injection of 100 mg kg^{-1} ALA (Egger *et al* 1996). Levels increased 50-fold (to 60 μg ml^{-1}) during the first hour after injection and declined to 30 μg ml^{-1} over the next 7 hours. Porphyrin production, as measured by fluorescence, increased only gradually in tissues with the highest levels in the liver after 8-10 hours, followed by the prostate, muscle, bladder, and skin. Several other studies have been performed examining the tissue distribution of ALA-derived PpIX following systemic administration (Peng *et al* 1992, Bedwell *et al* 1992, Fukuda *et al* 1993, Hua *et al* 1995, Henderson *et al* 1995). Although both oral and intravenous administration of ALA result in similar biodistribution kinetics, higher oral ALA doses are required to produce the same amount of PpIX as produced following intravenous administration because of presystemic drug elimination (first-pass metabolism) occurring in the intestinal lumen, gastrointestinal wall, and liver (Loh *et al* 1993).

Several patient studies have been conducted examining toxicity effects after ALA administration. Reports of patient nausea and vomiting have been made following the oral administration of varying ALA doses (Loh *et al* 1993, Webber *et al* 1997, Tope *et al* 1998, Gossner *et al* 1999, Ackroyd *et al* 1999, Hinnen *et al* 2000). In addition, transient liver abnormalities (elevated bilirubin, transaminases, and alkaline phosphatases) have been observed (Loh *et al* 1993, Webber *et al* 1997, Tope *et al* 1998, Ackroyd *et al* 1999, Gossner *et al* 1999). In general, cutaneous phototoxicity or abnormal neurological function was not reported. PpIX concentrations in the plasma varied widely among

patients (in the above studies) but appeared to be a function of dose (higher concentrations occurring earlier following higher doses).

Recent *in vivo* studies of photosensitizer uptake in different brain tumor models have supported the use of ALA in PDT (Hebeda *et al* 1998, Lilge and Wilson 1998, Olivo *et al* 1998, Stummer *et al* 1998c). Lilge and Wilson (1998) reported a significantly reduced uptake of ALA in white matter as compared to grey matter using the VX2 tumor (derived from a rabbit Orycytolagus cuniculus tumor of unspecified tissue origin) in rabbits. The lack of PpIX production in the white matter is likely attributed to the absence of heme synthesis in this tissue (Verma *et al* 1993). Despite a lower concentration of PpIX in both white and grey matter after 24 hours as compared to 6 hours, the tumor-to-grey matter uptake ratio was nearly identical at both times suggesting similar synthesis and clearance kinetics. Furthermore, a 100:1 tumor-to-white matter PpIX uptake ratio was reported following 100 mg kg^{-1} ALA administration. Since the tumor-to-white matter threshold dose value ratio was less than 0.02, the light fluence would need to be about 5000 times higher in white matter than in the tumor to cause equivalent damage. Olivo *et al* (1998) also found a greater PpIX production in grey matter than white matter using the VX2 tumor in rabbits. These findings strongly support the use of ALA in brain tumor treatment since the majority of adult tumors develop in the white matter. The superior selectivity would result in little or no photodamage to white matter, thereby preventing potentially debilitating neurological detriment. Tumor-to-normal tissue PpIX fluorescence in the C6 glioma tumor has been reported to be at least 6:1 six hours after ALA administration (Stummer *et al* 1998c).

ALA is a small, water-soluble molecule. Its ability to pass the blood-brain barrier (BBB) is currently the subject of dispute. By injecting ^{14}C-labelled ALA, Terr and Weiner concluded that the BBB is virtually impermeable to ALA following systemic (intravenous) administration (Terr and Weiner 1983). Shortly after ALA injection ^{14}C-labelled ALA was found only in areas of the brain that lacked BBB function and cerebrospinal fluid (CSF). Conversely, McGillion reported a blood level dependence of ALA concentrations in rat brain homogenates (McGillion *et al* 1974, McGillion *et al* 1975). However, ALA extraction after brain tissue homogenization does not allow the distinction of areas with intact BBB from areas with disrupted BBB (Hebeda *et al* 1998). Using autoradiographic techniques, quantitative studies have shown BBB permeability within tumor tissue and partial BBB permeability in brain adjacent to tumor (BAT) (Hasegawa *et al* 1983, Yamada *et al* 1982). Therefore, the ability of ALA to cross the intact BBB might not be of as much importance as imagined. Since PDT would be performed after surgical tumor removal, the BBB would be disrupted and ALA would freely permeate remaining tumor tissue in the resection margin. However, as previously mentioned, only partial BBB permeability exists in BAT. Tumor cells nested beyond the resection margin could be more resistant to ALA-mediated PDT because of the partial BBB permeability surrounding these cells. Furthermore, BBB regeneration following surgery could preclude the use of ALA in repeat PDT treatments if ALA cannot pass intact BBB. The development of lipophilic photosensitizers (ALA esters) might overcome this issue altogether if esters can penetrate the intact BBB (as would be expected from lipophilic compounds). However, a drawback associated with systemic h-

ALA administration pertains to liver toxicity. The toxicity of h-ALA is higher than ALA at comparable doses.

1.1.5 Light Delivery

Following the accumulation of PpIX in tumor tissue, the aim of PDT is to effectively destroy malignant cells by light irradiation. The penetration of light into tissue determines the extent of damage and is influenced by the wavelength of light and tissue type (Popovic *et al* 1995). Light transmission in brain parenchyma increases from 350 nm to 750 nm after which a plateau is observed (Popovic *et al* 1995). Due to the fact that porphyrins and PpIX exhibit light excitation energies of 630 nm, red light is most commonly used. However, the penetration depth of this wavelength light is only 1.5 mm in normal brain tissue and 2.9 mm in tumor tissue (Muller and Wilson 1985).

The benefits of fractionated dose delivery in PDT have been well documented. The general premise of fractionated treatment involves the re-oxygenation of target tissues. During a single, continual dose delivery, oxygen is depleted rapidly from the target tissue. However, fractionating the dose allows tissues to replenish oxygen levels, thereby enhancing the subsequent treatment. PDT experiments involving human glioma spheroids indicate that low fluence rates (longer treatment time) produce a greater cell kill than high fluence rates (Madsen *et al* 2001). Furthermore, the results of clinical trials suggest that improved patient prognosis is directly correlated with higher fluences (Muller and Wilson 1996).

1.2 Intent of Current Work

Primary malignant brain tumors account for 2-3% of the entire cancer burden and are the third leading cause of cancer deaths in the 15-35 year old age group (Black 1991). The most aggressive brain tumors are of the glial variety, specifically glioblastoma multiforme (GBM). GBM tumors exhibit a rapidly invasive, yet diffuse growth pattern that precludes effective treatment. Current treatment methods involve surgery, chemotherapy, and radiation therapy. Chemotherapy and radiation therapy focus on post-surgical treatment of tumor cells remaining in the resection margin. The benefits of radiation therapy treatment methods have been reported (Anderson 1978, Kristiansen *et al* 1981, Walker *et al* 1978, Walker *et al* 1980) but survival rates rarely improve significantly. Typical treatments involve fractionated dose delivery with doses of 1.8 - 2.0 Gy per fraction delivered to a total of 52 - 64 Gy. While increasing the dose may improve patient prognosis, it is unadvisable to do so because of the resulting detriment from normal tissue necrosis and leucoencephalopathy (Emami *et al* 1992, Fine 1994).

Chemotherapy has been explored as a brain tumor treatment method. Issues pertaining to delivery and tumor cell resistance have hampered the efficacy of chemotherapy. Systemic administration results in the death of cancer cells as well as healthy, normal cells. Attempts have been made to deliver the drugs intra-arterially to localize the treatment but the complexity of this procedure makes it undesirable. Furthermore, this technique can also result in unpredictable spatial distributions and significant concentration variations at the treatment site (Groothuis 2000).

Due to the many inadequacies of current GBM treatment methods, recent work has focused on developing a more aggressive focal treatment. Several aspects of PDT make

it a desirable treatment method (namely tumor selectivity, the possibility for repeat treatments, and the absence of treatment resistance). Current research is aimed at the development of: improved photosensitizers (such as ALA esters), light delivery devices, and more accurate PDT dosimetry techniques.

The use of ALA in neurosurgery has been limited to the field of photodynamic detection (PDD). Successful studies of ALA-mediated PDD have been reported (Stummer *et al* 1998a, Stummer *et al* 1998b, Stummer *et al* 2000, Stummer and Baumgartner 2000). Following tumor debulking, the resection cavities were irradiated with light resulting in visible PpIX fluorescence. The fluorescence further assisted micro-surgical tumor removal. Results were promising, prolonging patient survival for up to six months. The overall impact of PDD on patient survival, however, is limited by the difficulties associated with removal of infiltrative tumor. Although PDD allows accurate tumor visualization, it is often difficult to remove the infiltrative tumor tissue without compromising healthy neural tissue. It is often necessary to leave a margin of 7infiltrate to prevent adverse neurological deficit. The ultimate goal of PDT is to eliminate the infiltrate.

Few clinical PDT trials have been performed and those that have been conducted primarily involved HpD or Photofrin. Initial results were promising, however, treatment failure occurred in nearly all cases. The lack of success was likely due to the intra-operative singe dose treatment rather than successive, fractionated treatments.

The specific aim of this project is to examine the distribution of ALA and h-ALA-induced PpIX in a unique animal model in which tumors accurately represent GBM in patients. All previous *in vivo* GBM studies have been performed on animals possessing

cell line-derived tumors. Some of the most commonly used cell line-derived tumors are derived from the U-87MG (malignant glioma) line. Although glioma in origin, these cell line-derived tumors grow as solid masses *in vivo* rather than diffusely and invasively. The development of an accurate tumor model has permitted the *in* vivo study of ALA and h-ALA localization and PpIX quantification in authentic glioma tissue.

1.3 Significance of the Study

Current *in vivo* brain tumor research models are somewhat limited and restricted when examining photosensitizer pharmacokinetics because of the type of tumors employed. Cell line-derived tumors lack the diffuse and infiltrative growth pattern associated with GBM in patients and, therefore, may not accurately represent photosensitizer uptake and distribution. Although ALA-induced PpIX uptake and distrubtion has been explored *in vivo*, this study is unique in that fluorescence microscopy has never before been used to quantify tumor uptake of ALA and h-ALA photosensitizers in a biopsy tumor model. Foundational toxicity data will be obtained that can be used as standards for future *in vivo* studies. The examination of *in vivo* ALA and h-ALA distribution will provide valuable information regarding the potential of these photosensitizers in the clinical treatment of malignant gliomas.

1.4 Definition of Terms

Fluorescence is the direct result of the light activation of protoporphyrin IX (PpIX), not the exogenously administered prodrug (ALA). However, when discussing tumor selectivity, it is implied that the location of PpIX fluorescence reflects the location of

exogenously administered compound. Regarding selectivity, the terms PpIX and either ALA or h-ALA may be used interchangeably.

CHAPTER 2

METHODOLOGY

2.1 Photosensitizing Compounds

5-Aminolevulinic acid hydrochloride and the h-ALA were provided by PhotoCure (Oslo, Norway) in lyophilized form. Both compounds were dissolved in sterile saline (0.9% NaCl) by thorough mixing. Although it is often recommended that esters be initially dissolved in DMSO to facilitate adequate solubility (due to their hydrophobic chemical nature), this step was found to be unnecessary for homogenous solution production (possibly due to high compound purity). The lipophilicity of ALA and h-ALA is reflected by the octanol/water partition coefficients (P) as shown in Table 1. The h-ALA compound is roughly three orders of magnitude more lipophilic than ALA.

The effects of ALA acidity were examined by injecting ALA with unadjusted pH (pH ≈ 2.5), and adjusted pH of 5 and 7 into the rat brain. Results suggested that unadjusted ALA was unfavorable for local administration (see Chapter 3). Due to the acidity of ALA and the sensitivity of neural tissue, it was determined that the pH of ALA should be altered prior to local injection. Therefore, following compound preparation; the pH of ALA was adjusted using 10M and 1M NaOH in a drop-wise manner until a pH of 7 was obtained. Several studies have demonstrated the relative instability of ALA at neutral pHs (Bunke *et al* 2000, Novo *et al* 1996). ALA is a member of α-

amino ketones that dimerize readily in alkaline (basic) conditions (Krems and Spoerri 1947). The color change of ALA aqueous solutions (clear at low pH and transparent yellow at higher pH) (Chang *et al* 1996) was also observed in this experiment following compound neutralization. Due to this increased instability of ALA the compound was prepared immediately prior to use (1-2 hours). As a further precaution, the adjusted ALA was stored on ice as increased temperature may contribute to compound instability (Chang *et al* 1996). ALA stability was gauged qualitatively by visually noting any color change following solution preparation. The pH of h-ALA is approximately 5.5 and was therefore not altered prior to injection.

2.2 Cell Cultures

Human GBM biopsies were received and processed as quickly as possible following tumor removal to ensure tissue viability. Processing involved thorough mincing of tissue with a scalpel. Minced tissue was washed with Dulbecco's Modified Eagles Medium (DMEM) supplemented with 10% fetal calf serum, glutamax, and four times the prescribed concentration of non-essential amino acids (16 mL total in 500 mL of medium volume), then passed through 400 μm sterile mesh filters. Unfiltered tissue was further minced and washed. The washing and filtering process was repeated until all tissue passed through the filter. The filtrate was mixed thoroughly in 50 mL DMEM and 5 mL aliquots were dispensed into 80 cm^2 agar-coated culture flasks. The agar-overlay volume was composed of 15 mL DMEM supplemented with 10% heat-inactivated fetal calf serum, four times the prescribed concentration of nonessential amino acids (16 mL total), 2% L-glutamine, penicillin (100 IU mL^{-1}), and streptomycin (100 μg mL^{-1}). An

additional 10 mL of DMEM was added to each flask. Flasks were stored in a standard tissue culture incubator (37°C, 95% air, 5% CO_2, and 100% relative humidity) and medium was changed every 3 to 4 days. Spheroid development typically spanned 10 to 14 days after which time spheroids were prepared for injection. Optimal tumor induction is obtained by injecting ideally sized spheroids (250-350 μm) into the rat brain. Spheroids smaller than 250 μm contain too few cells and thus limit tumor-inducing capability. Diameters larger than 350 μm, however, also adversely affect tumor induction because of a necrotic spheroid center. As spheroids develop, the inner cells are gradually deprived of oxygen due to limited oxygen diffusion into the central region of the spheroid. Consequently, the tumor-inducing capability of large spheroids is less than optimal. Spheroids were sized by performing a series of filtrations with 250 μm and 350 μm mesh filters. The spheroids were first passed through a 350 μm filter. The un-filtered material was discarded (ie. spheroids larger than 350 μm). The filtrate was passed over a 250 μm mesh filter and spheroids contained on the filter (ie. sized greater than 250 μm but less than 350 μm) were retained. Sized spheroids were then transferred from the filter paper surface to a petri dish with agar medium. To ensure spheroid viability the animal injections were performed within two hours of spheroid sizing.

For comparative purposes, animals were also injected with cells from the U-87MG cell-line (originally derived from a malignant glioblastoma astrocytoma in a female patient by explant technique). Cells were cultured in DMEM, flasks were stored in a standard tissue culture incubator (37°C, 95% air, 5% CO_2, and 100% relative humidity), and medium was changed every 3 to 4 days. Cells were grown to 75% confluence after which time DMEM medium was removed and cells were detached from the flasks by a 3-

minute incubation with 0.01 M trypsin/EDTA (ethylenediamine tetraacetic acid). The chelating activity of EDTA was inactivated by the addition of DMEM. Cells were suspended in medium and centrifuged for 5 minutes at 836 times gravity (Heraeus Sepatech Megafuge 1.0, rotor #2705, 1000 rpm). The supernatant was removed and the pellet was re-suspended with 500 µL of medium. A 50 µL aliquot was removed for cell counting.

While a direct comparison between biopsy tumors and cell-line tumors would be best performed by injecting spheroids in both experiment types, it was determined that $1x10^6$ U87-MG cells would be injected for cell-line tumor induction, to enhance experiment expediency. As mentioned, spheroid development spans 3 to 4 weeks whereas cell culture maturation can occur in less than a week. Furthermore, no histopathological differences have been observed between tumors established from single-cell suspensions and spheroids (Engebraaten *et al* 1999).

2.3 Animal Experiments

Nude rats (Han: *rnu/rnu* Rowett) were used in these experiments. To allow tumor development, immuno-deficient rats were required. A fully functional immune system typically precludes cross-species transplantation due to the immune system's capability to effectively destroy histo-incompatible tissue (xenotransplantation). Animals were kept in a specific pathogen-free environment (25°C), in positive-pressure rooms with filtered and humidified air (55% relative humidity) on a standard 12-hour day/night cycle. Animals aged 4 to 5 weeks, weighing 60 to 80 g, were used in these experiments. Anesthetization was performed by subcutaneous injection of 0.1 mg kg^{-1} fentanyl, 5 mg kg^{-1} fluanison,

and 2.5 mg kg^{-1} midazolam. Control animals were injected with Phosphate Buffered Saline (PBS).

2.3.1 Photosensitizer Toxicity

Following anesthetization, the rat's head was immobilized in a stereotactic frame. A rod was inserted into each of the outer ears and a nose clamp was applied to prevent skull movement. The automated injection apparatus was coupled to the stereotactic frame to maintain precision during injections. Once immobilized, a 5-7 mm longitudinal incision was made in the scalp. Using a dental drill (2 mm drill bit diameter), a burr hole was created 1 mm laterally (right) to the midline fissure and 1 mm posterior to the frontal fissure in the animal's skull. The canula was lowered to a depth of 2.5 mm below the surface of the brain and the 30 μL photosensitizer-containing volume was injected over a 3-minute time period.

Photosensitizer concentration ranges of 10-398 mM ALA and 6.6-265 mM h-ALA were used to determine the maximum tolerable dose for topical drug administration in the Rowett nude rat. Respiratory distress leading to death is the main observable side-effect following high dose administration of these drugs. As such, labored breathing was noted during and after photosensitizer injection. A total of 40 rats were injected – 6 systemically (intraperitoneal) and 34 locally (Table 2).

2.3.2 Tumor Induction

Animal preparation and immobilization was performed as described in Section 2.3.1. Following the creation of a burr hole, the canula was lowered to a depth of 2.5 mm below the dura and the 30 μL spheroid-containing or cell-containing volume was injected over a 3-minute time period. A total of 10 spheroids in the 30 μL volume were injected. For

cell-line experiments, one million cells were injected (equivalent to the tumor-inducing ability of 10 spheroids). The canula was slowly withdrawn to prevent spheroid or cell backflow and the incision was closed. Rats were monitored daily for neurological detriment exhibited through abnormal gait and/or behavior. Abnormal behaviors were considered to be attributed to the tumor and, therefore, were equated with mature development. Spheroid-induced tumors required at least 3 months for complete development (resulting in neurological impairment) whereas cell-line tumors developed fully in 2 or 3 weeks.

Table 2 Toxicity Experiments

Compound	Administration Method	Concentration or Volume	Number of Animals
ALA	Systemic (IP)	119 mM	2
	Local (intracranial)	398 mM	2
		199 mM	8
		99 mM	2
		20 mM	2
		10 mM	2
H-ALA	Systemic (IP)	79 mM	2
	Local (intracranial)	265 mM	2
		132 mM	8
		66 mM	2
		13 mM	2
		6.6 mM	2
PBS	Systemic (IP)	100 µL	2
	Local (intracranial)	30 µL	2
Total Animals			40

2.3.3 Photosensitizer Uptake

After a sufficient tumor growth period, photosensitizer injections were performed to quantify the PpIX production in tumor cells. Again, animal preparation, immobilization, and compound injection were performed as described in Section 2.3.1. Based on toxicity

studies (Section 2.3.1) the ALA and h-ALA concentration for intra-tumoral injection was determined to be 99 mmol L^{-1} ALA and 66 mmol L^{-1} h-ALA. A total of 47 rats (excluding h-ALA titration experiment) were injected intra-cranially with this dose of ALA and h-ALA. Table 3 summarizes the photosensitizer uptake experiments.

Table 3 Photosensitizer Uptake Experiments

Tumor Type	Compound	Administration Method	Concentration or Volume	No. of Animals
Biopsy	ALA	Local	99 mM	7
		Systemic	125 mg kg^{-1}	9
	H-ALA	Local	66 mM	7
		Systemic	50 mg kg^{-1}	11
	PBS	Local	30 µL	4
		Systemic	100 µL	2
U-87MG	ALA	Local	99 mM	7
	H-ALA	Local	66 mM	6
	PBS	Local	30 µL	2
Total Animals				55

In two separate experiments, a total of 20 rats were injected systemically (intra-peritoneally) with ALA and h-ALA. In the first experiment, 9 rats were injected with 125 mg ALA per kg body weight and 1 rat was injected with PBS. In the second experiment, 9 rats were injected with 50 mg h-ALA per mg body weight and 1 rat injected with PBS. In each experiment, the 9 rats that received photosensitizer were divided into three time groups. The first group was sacrificed after 1 hour of photosensitizer incubation, the second group was sacrificed after 4 hours, and the third group was sacrificed after 6 hours. In a separate, related experiment, 2 rats were injected with 50 mg h-ALA per mg bodyweight each and sacrificed after 4 hours (these rats displayed signs of neurological impairment and were therefore required to be sacrificed).

Two h-ALA titration experiments were conducted to determine the effect of varying photosensitizer concentration on the PpIX production in tumor cells following topical administration (outlined in Table 4). The first experiment consisted of 6 rats (three groups). Two rats in the first group received 13 mM, both rats in the second group received 33 mM, and both rats in the third group received 66 mM. The second experiment involved 14 rats (separated into 5 groups). Three rats in the first group were given 13 mM, three rats in the second group received 33 mM, and 66 mM h-ALA was administered to the third group. The fourth group was given 99 mM ALA for comparative purposes. The fifth group consisted of PBS controls (30 μL injection).

Four hours after injection the animals were sacrificed and the intact, whole brains were removed in dark conditions (red light) to prevent photobleaching of neural tissue. The tissue was cooled in TissueTek® (Bayer Corporation, Pittsburg, PA, U.S.A.; Cat. No. 4583) on dry ice before "halving" the brain. A section was made in the coronal plane along the canula tract to separate one section for further sectioning and one section for macroscopic pathology examination (storage in 4% formalin). The frontal section was frozen completely in TissueTek and stored at -70°C until microtome sectioning. Sectioning was performed in dark conditions to prevent photobleaching. The tissue samples were sectioned in 10 μm thick slices to allow a greater amount of PpIX fluorescence during microscopy. Typical tissue sample thickness for conventional microscopy ranges from 5-8 μm.

Table 4 Titration Experiment in Biopsy Tumors

Compound	Administration Method	Concentration or Volume	Number of Animals
H-ALA	Local	13 mM	5
		33 mM	5
		66 mM	5
ALA	Local	99 mM	3
PBS	Local	30 μL	2
Total Animals			20

2.4 Microscopy & Quantification

Fluorescence microscopy was performed with a biological research microscope (Nikon model E800) with a 100-watt mercury vapor lamp. A highly photosensitive, thermo-electrically cooled charge-coupled device (CCD) camera was used to perform fluorescence imagery under the control of AquaCosmos software (1.20 version). The resolution of the images was 1280x1024 pixels with a dynamic range of 16 bits per pixel (ORCAII, Hamamatsu Photonics K.K., Japan). The filter combination used included a 380-420 nm excitation filter, a 430 nm beam splitter, and a 630±20 nm band-pass emission filter. For comparative purposes, digital images of corresponding Hematoxylin and Eosin (HE) stained samples were obtained (additional coronal section) to anatomically verify the presence of tumor tissue. Adequate fluorescence image development was found to result following a sample irradiation time of 15 seconds. The images were acquired under 4X magnification (the largest field of view).

Quantification was performed by manually selecting regions of interest (ROIs) in tumor tissue and normal tissue. Program analysis provided the maximum, minimum, and average pixel intensity within the ROI.

CHAPTER 3

RESULTS & DISCUSSION

3.1 Toxicity Study

Results of the toxicity experiments involving non-tumor bearing rats are summarized in Table 5. As illustrated, survival appears to be dependent on the type of anesthetizing agent used. For example, 8 of the 10 animals subjected to Halothane died. The findings that all 4 rats in the 199 mM ALA group died following Halothane anesthetization compared to 1 of 4 deaths after Enfluran anesthetization, and 3 of 4 deaths in the 132 mM h-ALA group after Halothane compared to no deaths in the Enfluran group, strongly suggests anesthesia-induced death by malignant hyperthermia.

Based on the toxicity data it was determined that the maximum tolerable ALA and h-ALA doses for local, intra-cranial injection are 99 mM and 66 mM, respectively. Although only one animal died in the 199 mM ALA group, and no deaths occurred in the 132 mM h-ALA group (following Enfluran anesthetization), some animals experienced breathing difficulties. As a result, 99 mM ALA and 66 mM h-ALA doses were deemed safe. The single death in the 99 mM ALA group was attributable to the animal's low body weight.

Table 5 Results of Toxicity Experiments

Compound[a]	Administration Method	Anesthesia	Description of Result
ALA (119 mM)	Systemic	Enfluran	2 of 2 rats lived
ALA (398 mM)	Local	Enfluran	2 of 2 rats died during injection
ALA (199 mM)	Local	Enfluran	1 of 4 rats died after injection (respiratory distress)
ALA (199 mM)	Local	Halothane	All 4 rats died
ALA (99 mM)	Local	Enfluran	1 of 2 rats died after injection (low body weight)
ALA (20 mM)	Local	Enfluran	2 of 2 rats lived; 1 rat experienced respiratory distress
ALA (10 mM)	Local	Enfluran	2 of 2 rats lived
h-ALA (79 mM)	Systemic	Enfluran	2 of 2 rats lived
h-ALA (265 mM)	Local	Enfluran	2 of 2 rats died during injection
h-ALA (132 mM)	Local	Enfluran	4 of 4 rats lived; 1 rat experienced respiratory distress
h-ALA (132 mM)	Local	Halothane	1 of 4 rats lived
h-ALA (66 mM)	Local	Enfluran	2 of 2 rats lived
h-ALA (13 mM)	Local	Enfluran	2 of 2 rats lived
h-ALA (6.6 mM)	Local	Enfluran	2 of 2 rats lived
PBS (100 µL)	Systemic	Enfluran	2 of 2 rats lived
PBS (30 µL)	Local	Halothane	1 of 2 rats lived

[a] ALA compound pH adjusted to neutral (pH 7) prior to local injection. The h-ALA compound was unadjusted (pH 5.5) for local and systemic injections.

In a small experiment involving 12 rats, the effects of varying ALA pH was studied. The unadjusted pH of ALA in solution is roughly 2.5. Injecting an acidic compound directly into neural tissue could have devastating effects. Four rats were injected with unadjusted ALA (99 mM) and eight rats were injected with pH-adjusted ALA (99 mM); four injected with pH 5 and four injected with pH 7 (neutral). The results are summarized in Table 6.

Table 6 Effect of Varying ALA pH

ALA pH	Number of Rats	Description
2.5 (unadjusted)	4	3 rats died shortly after injection
5	4	3 rats died shortly after injection
7 (neutral)	4	1 rat died shortly after injection

Based on the low survival rates at low pH (pH 2) and only one death at neutral pH, it was determined that the pH of ALA would be adjusted to neutral (pH 7) prior to local, intra-cranial injection. The reason for one death in the neutral pH group is unknown, however, it could be related to the depth of canula placement rather than compound pH. If the photosensitizer was injected too deeply (ie. into the brain stem) it may adversely affect respiration or cardiac function.

3.2 Cell-Line Tumors

3.2.1 Qualitative Image Analysis

Images of cell-line tumors following local injection of ALA generally showed a greater peripheral uptake of photosensitizer than in central tumor regions (illustrated in Figure 4). Associated with cell-line tumors is an encapsulating membrane produced as a physiological defense response to a foreign solid mass (tumor). The outward diffusion of ALA from the tumor center to the periphery is likely attributed to the compound's hydrophilicity. ALA accumulates and is retained at the tumor's edge because of its inability to cross the lipophilic encapsulation. This observed effect has relatively little clinical relevance because the aggressive tumors with which this project is concerned (GBM), do not exhibit the growth pattern of cell-line tumors. The use of such simple cell line models in the evaluation of experimental therapies such as PDT would likely result

in unrealistically high survival rates and would thus not be an accurate predictor of the outcome of clinical trials.

The administration of h-ALA in animals with cell-line tumors resulted in slightly different results than that observed following ALA administration. Figure 5 shows the relatively scattered PpIX production following the injection of h-ALA. Despite the diffuse fluorescence pattern, PpIX production appears to be localized entirely in the tumor. Figure 6 shows the relatively weak fluorescence signal obtained after only one hour of h-ALA incubation.

3.2.2 Quantitative Image Analysis

Rectangular ROIs were created in the central tumor area, the tumor periphery, and in normal tissue. Fluorescence quantification was performed in a total of 6 samples: 4 in the ALA group and 2 in the h-ALA group. Of the 4 ALA samples, 3 were derived from the same animal (ie. different slices from the same tumor as denoted by "a", "b", or "c"). As shown in Figure 7, PpIX production is relatively constant in tumor tissue, wheras larger variations are observed in normal tissue. The average tumor-to-normal tissue uptake ratio, as determined from the data in Figure 7, was found to be 4.4±2.5:1.

PpIX production following h-ALA injection was examined in only two cell-line samples (Samples 3 and 4, Figure 8). Normal tissue fluorescence was at background levels (auto-fluorescence) in Sample 3 but substantially higher in Sample 4. This is due to the fact that the PpIX accumulation time was limited to one hour in Sample 3 as opposed to six hours in Sample 4. Based on the data presented in Figure 8, tumor-to-normal tissue ratios following 1 and 6 hour h-ALA administration were 20±184:1 and 1.4±0.5:1, respectively.

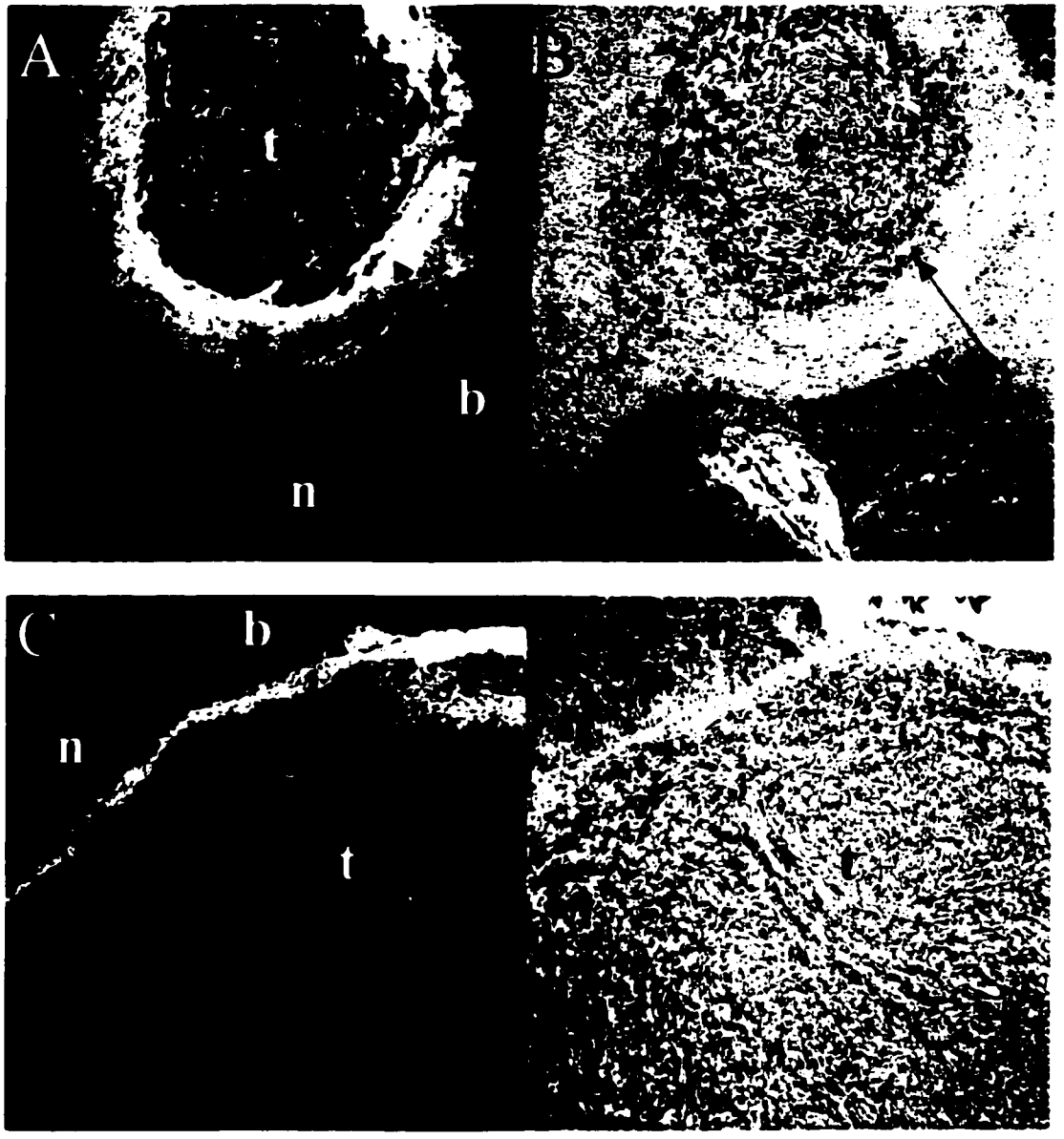

Figure 4. A, C: Four-hour ALA-induced PpIX fluorescence of U-87MG cell-line tumors (t) in the normal (n) rat brain. Note the sharply defined border (b) and PpIX accumulation. B, D: HE sections corresponding to (A) and (C), clearly reflecting tumor (t) area and tumor border (b) as well as the normal (n) tissue.

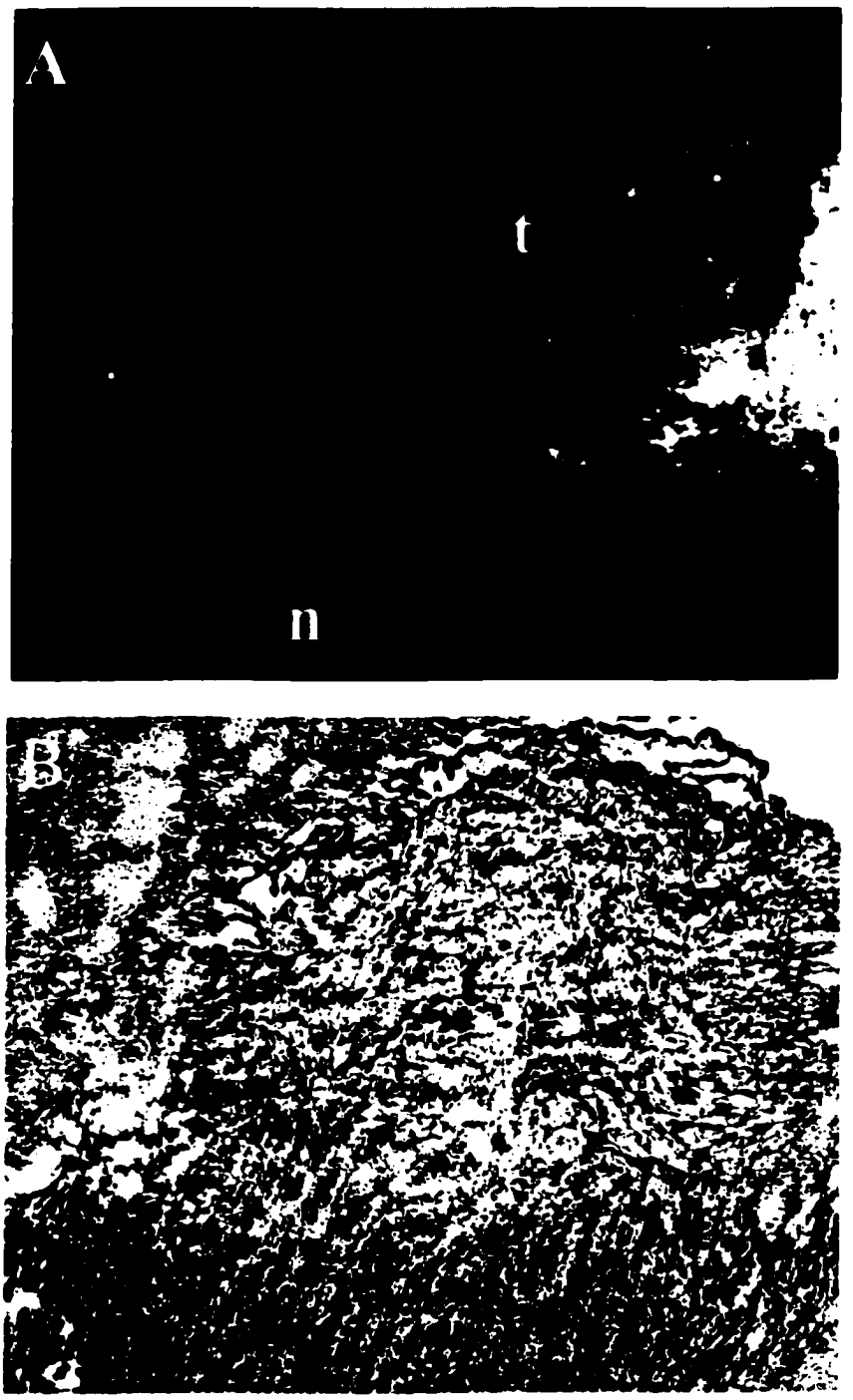

Figure 5. A: Six-hour h-ALA-induced PpIX fluorescence of a U-87MG cell-line tumor (t) in normal (n) rat brain. Note the patchy PpIX distribution in tumor. B: Corresponding HE section showing tumor (t) and normal (n) brain tissue.

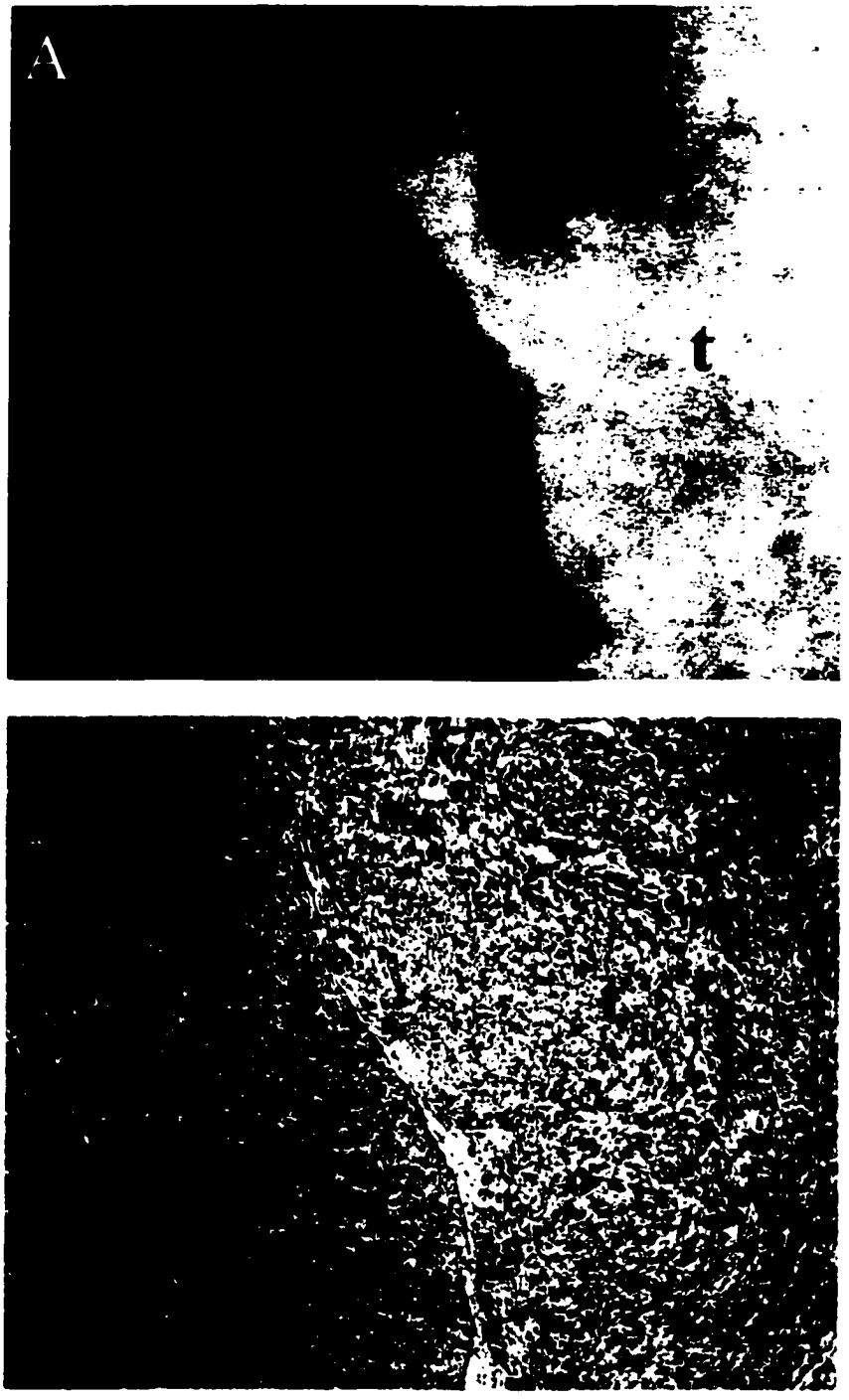

Figure 6. A: One-hour h-ALA-induced PpIX fluorescence of a U-87MG cell-line tumor (t) in normal (n) rat brain. Note the less relative PpIX fluorescence between tumor (t) and normal (n) tissue. Again, tumor border is well defined. B: Corresponding HE section showing tumor (t) and normal (n) brain tissue.

Tumor border fluorescence was measured in three different locations in each of the 4 samples (1a, 1b, 1c, and 2). The mean tumor border and normal tissue fluorescence are summarized in Figure 9. From the data in Figure 9, the average border-to-normal tissue fluorescence is 6.4±1.3:1. Since central tumor-to-normal tissue fluorescence is 4.4±2.5:1, nearly twice as much PpIX accumulates at the edge as in the center of cell-line tumors. Border fluorescence in the h-ALA samples was not measured due to a lack of visible accumulation at the tumor periphery.

The tumor-to-normal tissue PpIX fluorescence ratios for U-87MG cell-line tumors are summarized in Figure 10. The ALA, value of 4.4±2.5:1 is in quantitative agreement with Peng *et al* (unpublished)[†] who observed a tumor-to-normal tissue uptake ratio of 2:1 in basal cell carcinomas (BCCs), Xiao *et al* (1998) who reported uptake ratios ranging from 3:1 to 5:1 in a bladder tumor model, and Stummer *et al* (1998c) who reported 6:1 uptake in the C6 glioma tumor. Slight variations in uptake ratios from those observed by Peng *et al* may be due to the different tumor types studied. With regards to the h-ALA, only slight differences in PpIX fluorescence were observed in normal and tumor tissues (Figure 8).

It is interesting to note that there was essentially no PpIX fluorescence in normal tissues one hour following photosensitizer administration, however, weak tumor fluorescence was observed. This would seem to suggest that it might be clinically advantageous to consider PDT treatments with h-ALA shortly after administration (ie. 1 hour). It should be noted however, that due to the small sample size studied, it is difficult to reach definitive conclusions in this case. Further investigation is certainly warranted.

[†] Personal Correspondence

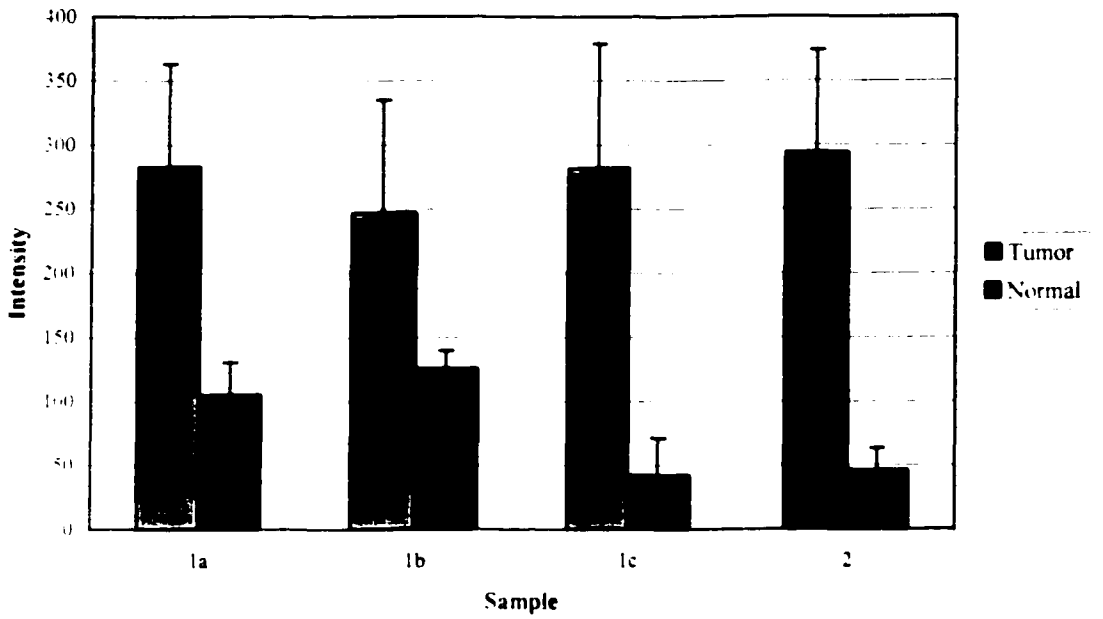

Figure 7. Relative ALA-induced fluorescence in U-87MG cell-line. Samples 1 and 2 were obtained four-hours after ALA administration.

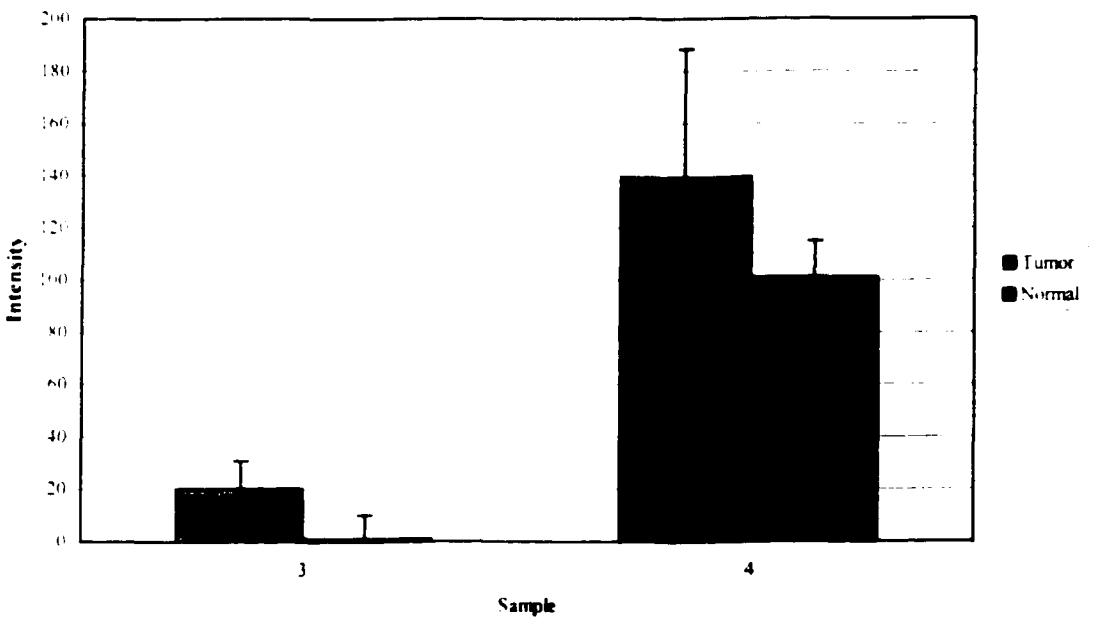

Figure 8. Relative h-ALA-induced fluorescence in U-87MG cell-line tumors. Sample 3 was obtained one hour after h-ALA administration. Sample 4 was obtained six hours after h-ALA adminstration

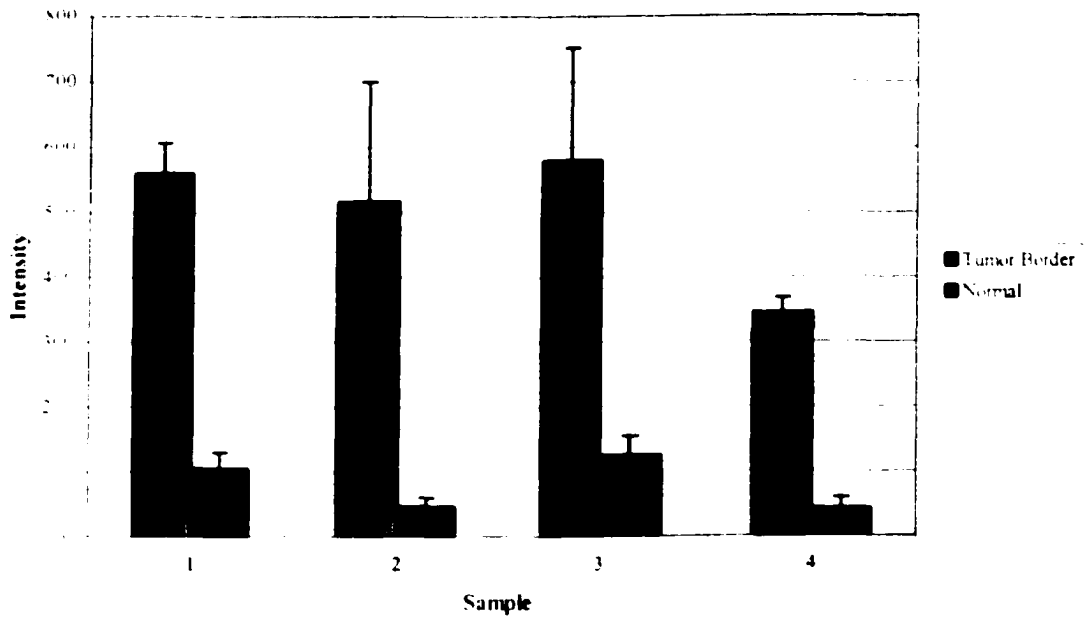

Figure 9. ALA-induced tumor border fluorescence in U-87MG cell line tumors (corresponding to the samples in Figure 7).

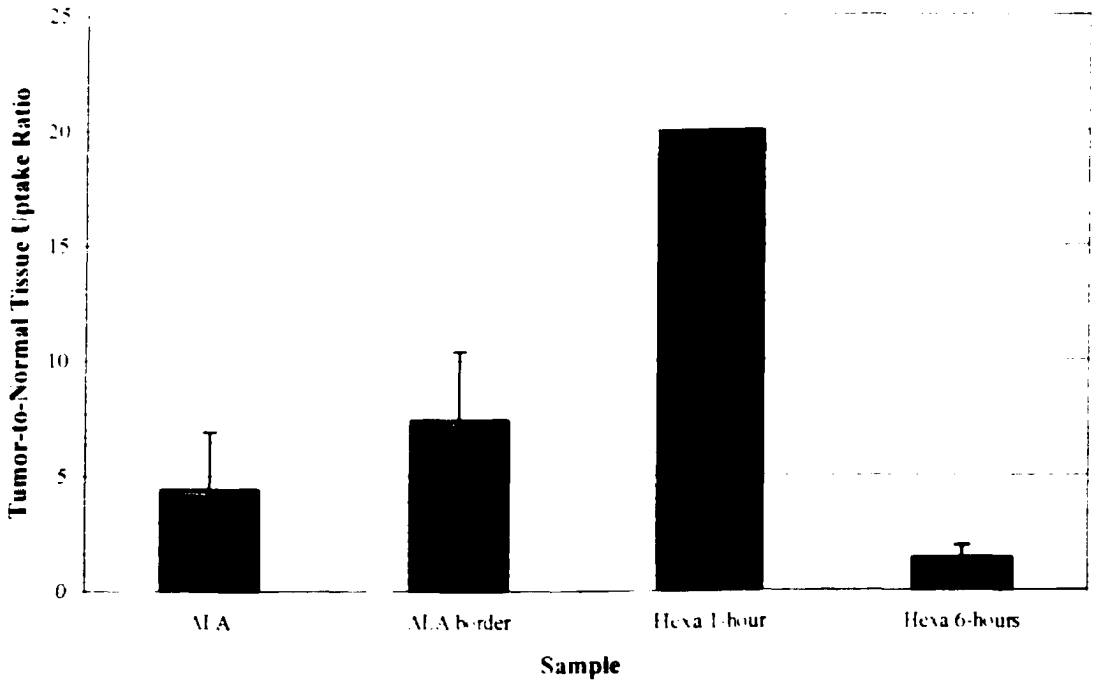

Figure 10. Tumor-to-normal tissue uptake ratios in U-87MG cell line tumors. Included are the average ALA-induced tumor uptake ratio, the average ALA-induced border uptake ratio, and the h-ALA-induced uptake ratios in 1- and 6-hour samples.

3.3 Biopsy Tumors

3.3.1 Qualitative Image Analysis

The invasive nature of GBM in the biopsy tumor model is clearly evident in both fluorescence images and HE sections. Fluorescence patterns show concentrated PpIX production in the central tumor and a gradual tapering of fluorescence with an increasing distance from the tumor's core. There is a good correspondence between the fluorescence images and the HE sections, the latter illustrating densely nucleated tumor cells gradually diminishing with distance from the center. Figures 11 through 13 illustrate this fluorescence pattern (resulting from ALA administration) and corresponding tumor physiology. These images clearly indicate the physical distinction between cell-line tumors and biopsy tumors and the superior mimicry of biopsy tumor to GBM in patients (see Section 3.3.1). Furthermore, photosensitizer distribution is markedly different in the two tumor types. PDT treatment efficacy in currently used tumor models (cell-line) may not accurately predict patient response to PDT in brain tumor treatments.

Biopsy-induced tumors typically possess a diffuse, infiltrative growth pattern. However, the growth pattern may vary somewhat from tumor-to-tumor and may be related to physiological properties of the biopsy from which it was obtained. For example, certain tumor borders may be well defined due to the tumor's proximity to obstructing anatomical structures (ie. corpus callosum or brain stem) whereas other areas of the tumor may disseminate gradually. As illustrated in Figures 13 and 14, h-ALA-induced PpIX fluorescence was confined primarily to tumor cells. In some cases, the

fluorescence was very diffuse (Figure 13), while in other instances, PpIX production was confined entirely to the tumor that exhibited well-defined borders (Figure 14).

3.3.2 Quantitative Image Analysis

Rectangular ROIs were drawn in central tumor areas and surrounding normal and/or diffuse tumor tissue. Fluorescence quantification was performed in a total of 10 samples. Of these 10 samples, 5 distinct tumors were represented. Three samples (5a, 5b, 5c) representing one tumor were examined following ALA administration. Figure 15 outlines the relative fluorescence of these samples. A fluctuation in PpIX production is evident with tumor-to-normal tissue uptake ranging from 4:1 (Sample 5a) to roughly 2:1 in samples 5b and 5c. However, fluorescence levels in the tumor itself remain relatively constant throughout the samples. This consistency is also seen in the U-87MG cell-line tumors. The fluctuation exists in the surrounding normal tissue and is the factor responsible for the uptake disparity. These results may be somewhat misleading due to the nature of biopsy tumors. The low tumor-to-normal tissue uptake in samples 5b and 5c is likely due to the presence of diffuse tumor infiltrate in the normal tissue ROI. Unfortunately, under 4X magnification it is often difficult to isolate normal tissue within the sample. It is conceivable that some fluorescence in normal tissue is the result of tumor invasion. Therefore, it is possible that ALA tumor uptake is superior to the uptake calculated in this study. From the data presented in Figure 15, the tumor-to-normal tissue uptake of ALA in biopsy tumors is 2.4±1.1:1. This tumor uptake corresponds with the 2:1 ratio reported by Peng *et al* (unpublished)[†] in BCCs and the 3:1 ratio reported by

[†] Personal Correspondence

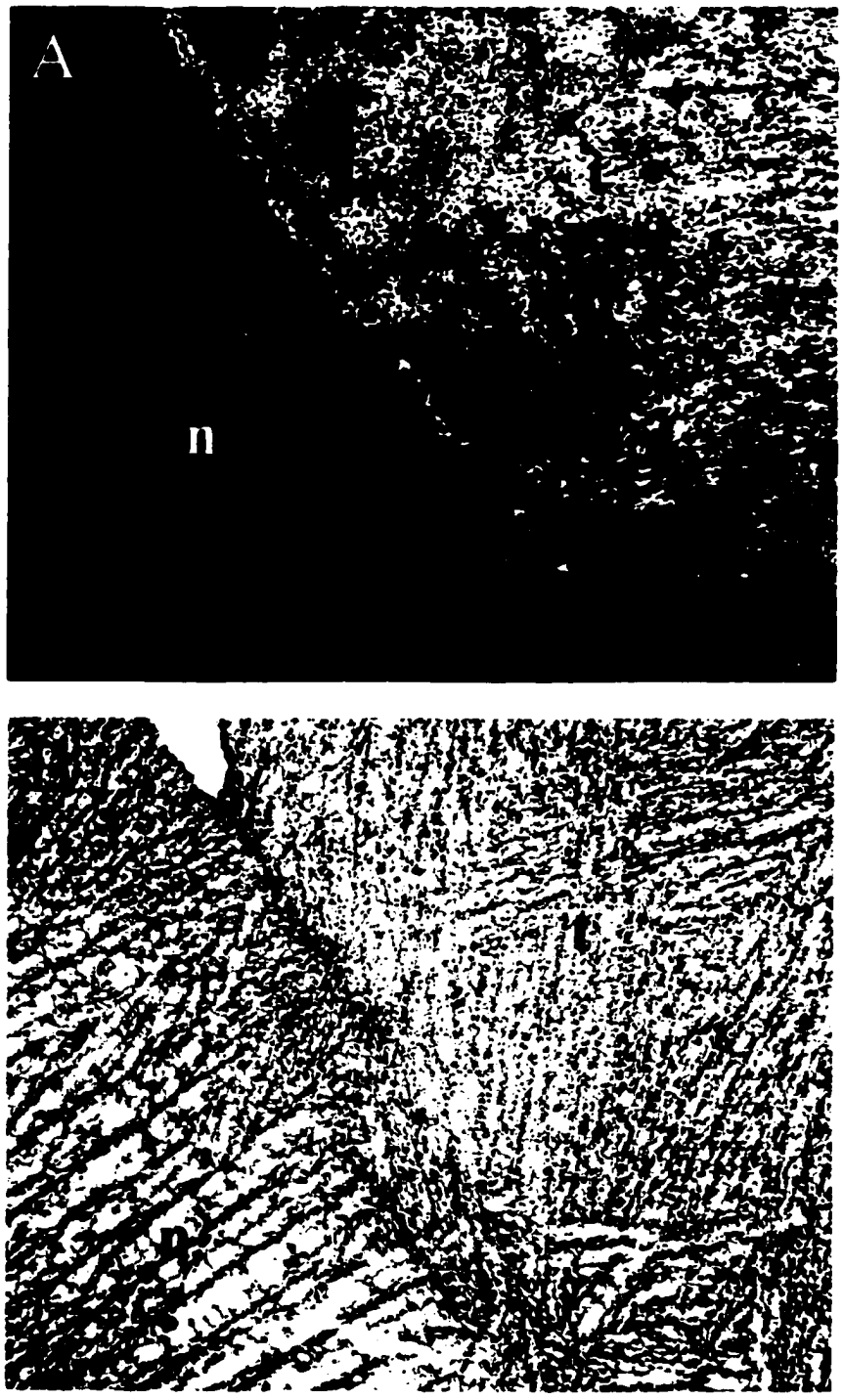

Figure 11. A: Four-hour ALA-induced PpIX fluorescence of a large biopsy-derived tumor (t) in normal (n) rat brain. Note the diffuse tumor infiltration into normal tissue as fluorescence gradually dissipates with increasing distance from the central tumor. B: Corresponding HE section illustrating tumor (t) tissue and normal (n) brain tissue.

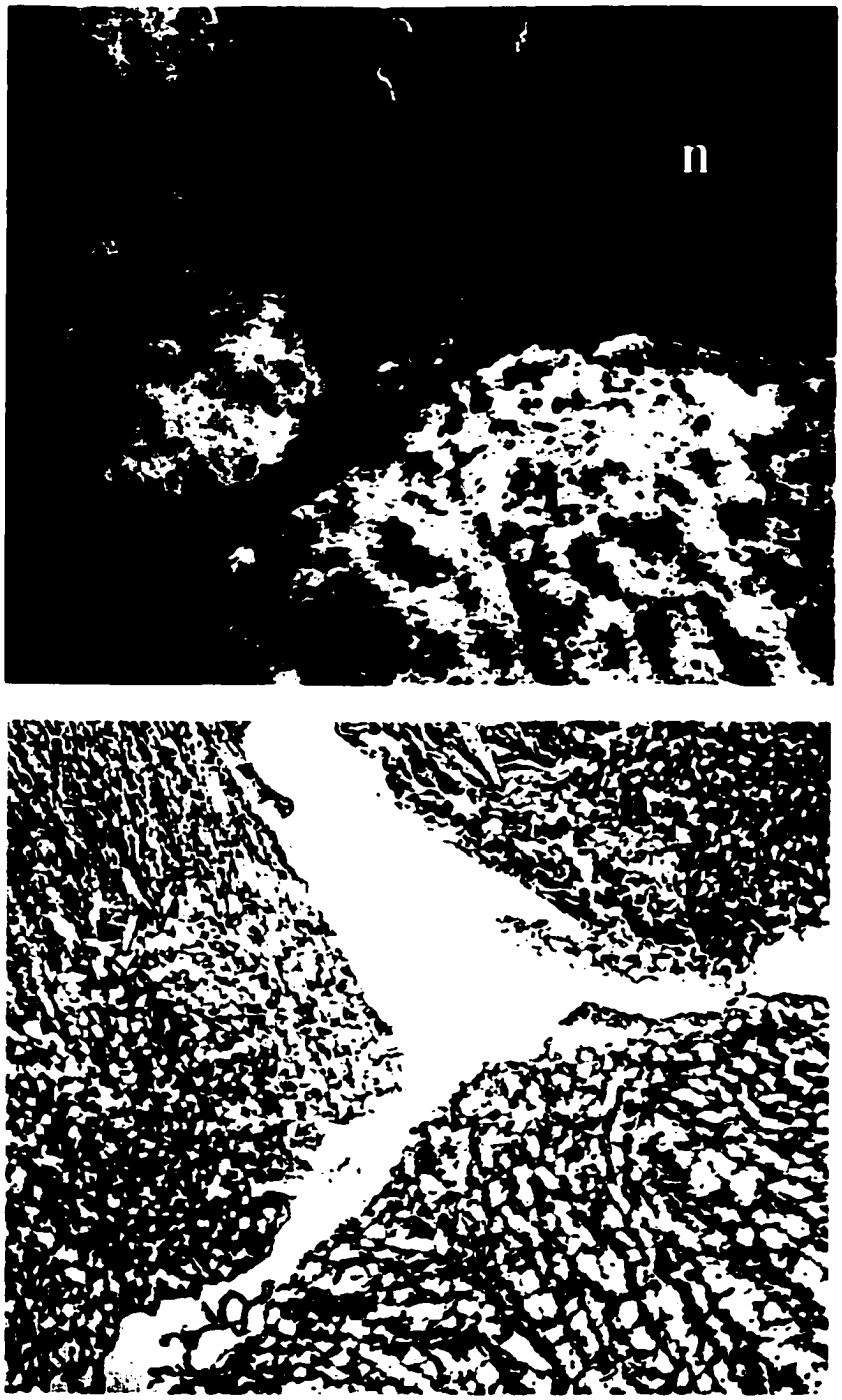

Figure 12. A: Four-hour ALA-induced PpIX fluorescence of a biopsy-derived tumor (t) in normal (n) rat brain. Note the non-homogenous fluorescence distribution in tumor as well as the large tumor border (b) area. B: Corresponding HE section reflecting tumor (t) tissue, the border area (b), and normal (n) brain tissue.

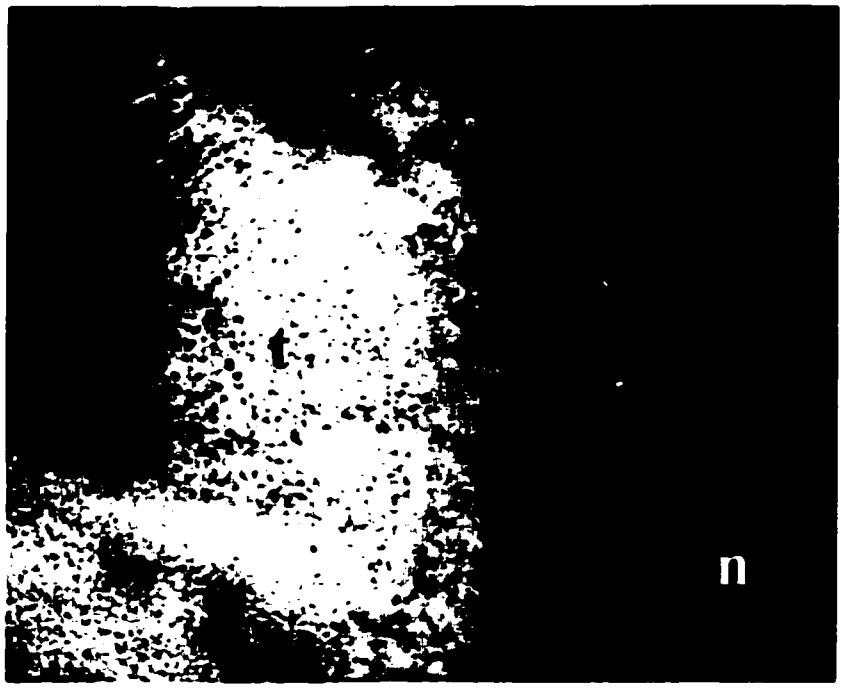

Figure 13. This photomicrograph is a typical representation of biopsy-derived tumors, illustrating gradual tumor diffusion/invasion (b) into normal (n) tissue as h-ALA-induced PpIX fluorescence dissipates gradually from the central tumor (t) area.

Xiao *et al* (1998) in bladder tumors. However, the calculated uptake ratio is slightly lower than results reported by Stummer *et al* (1998c) and Lilge and Wilson (1998). Stummer *et al* reported an ALA tumor uptake of at least 6:1 in C6 glioma tumors (6 hour peak) while Lilge and Wilson found ALA concentrations to be 100 times higher in VX2 tumors than in surrounding white matter.

The primary attraction for ALA use relates to its superior tumor-to-normal tissue selectivity, especially in white matter (Lilge and Wilson 1998). At this time, the specific origin of ALA selectivity is not known. However, the mitochondrial benzodiazepine receptor (MBR) has been implicated as a factor in ALA selectivity and, therefore, has been the subject of recent interest. Two different benzodiazepine receptors exist:

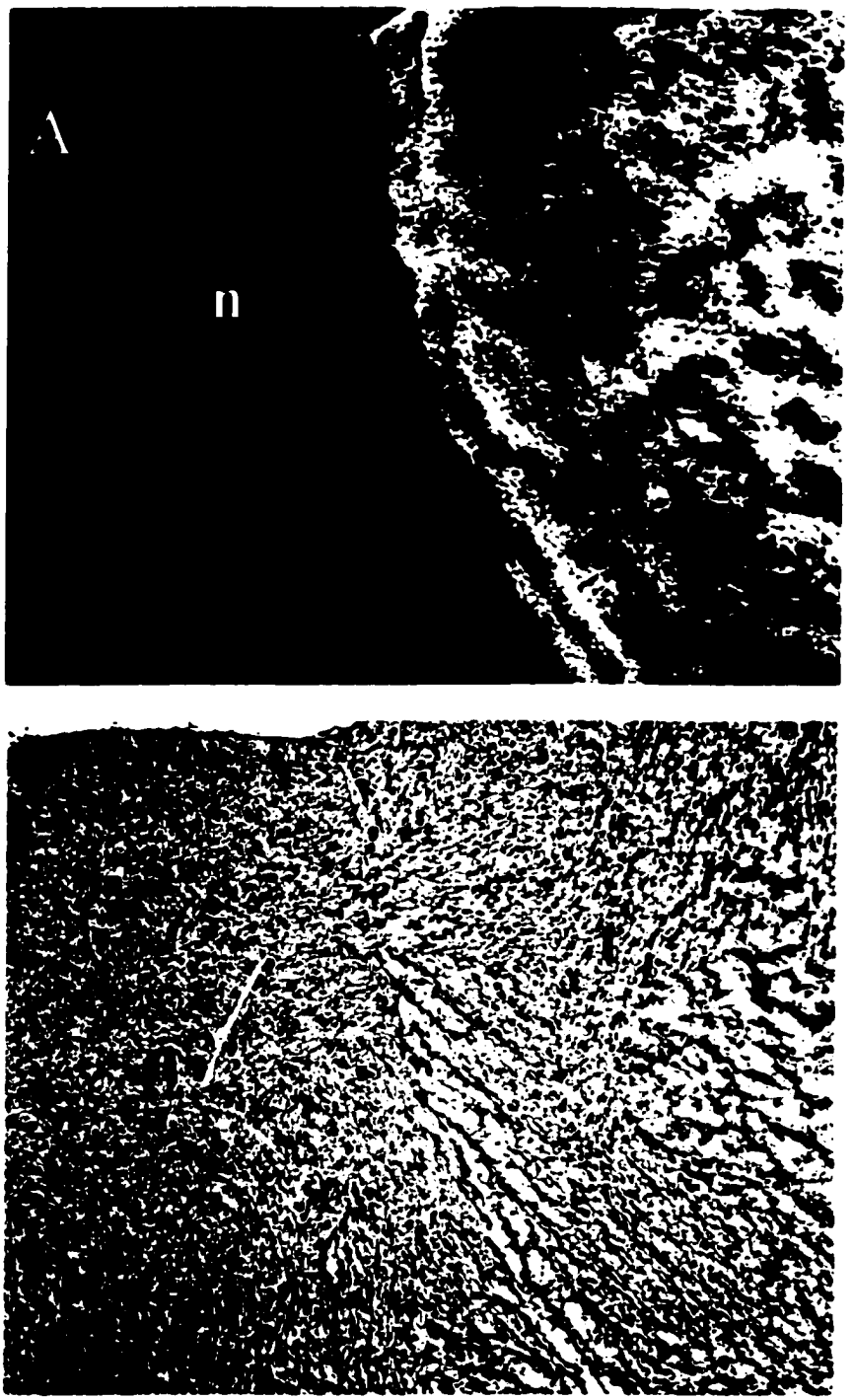

Figure 14. A: Four-hour h-ALA-induced PpIX fluorescence of a large biopsy-derived tumor (t) in normal (n) rat brain. In this case the border is very well defined. B: Corresponding HE section showing tumor (t) tissue in the normal (n) brain.

neuronal benzodiazepine receptors that are restricted to the brain and peripheral benzodiazepine receptors (PBR) that exist in peripheral tissues such as adrenal glands, liver, and kidneys. The PBR is localized in the outer mitochondria membrane and is therefore referred to as the MBR. MBR has a high affinity recognition site for PpIX and uses PpIX as an endogenous ligand (Pastorino *et al* 1994). Since PpIX is produced in the mitochondria it must traverse the inner and outer membrane. While the exact transport mechanism is not known, it is expected that MBR is the primary target for ALA or h-ALA-mediated PDT. It has been postulated that the frequency of apoptosis may be improved by inhibiting anti-apoptotic factors associated with the MBR. The inhibition of these anti-apoptotic factors in conjunction with ALA or h-ALA-mediated PDT could further improve treatment efficacy.

PpIX production following h-ALA administration was studied in 7 samples representing 4 different tumors (see Figure 16). The calculated relative fluorescence values are reported in Table 7. The average tumor-to-normal tissue uptake ratio of 7.6±2.0:1 also corresponds to a study by Peng *et al* (unpublished)†. Further, tumor-to-normal tissue uptake ratios are similar from sample-to-sample and tumor-to-tumor (despite a variation in PpIX levels in tumor tissue and normal tissue).

Results of fluorescence in biopsy tumors are summarized in Figure 17. The results show that the superior tumor-to-normal tissue localization observed with the h-ALA is due to very low levels of PpIX produced in normal tissue. As shown in Figure 17, PpIX levels in tumor tissue following ALA administration were not significantly different from that obtained following h-ALA administration. From a clinical standpoint, the low levels

† Personal Correspondence

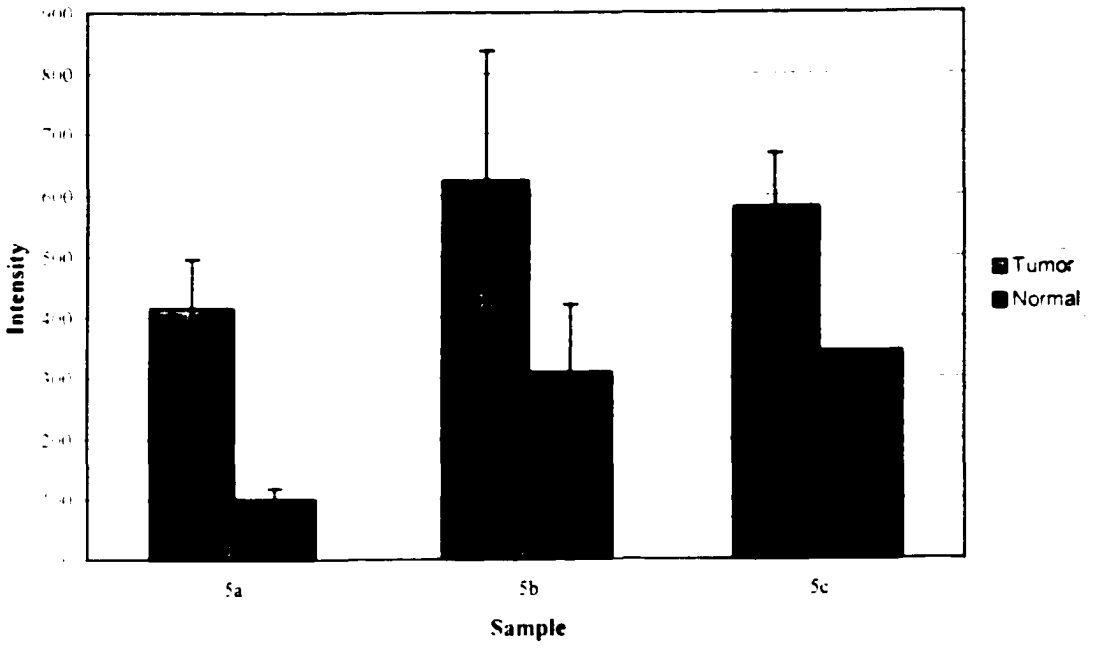

Figure 15. Relative ALA-induced fluorescence in biopsy tumor. Sample 5 was obtained four hours after ALA administration.

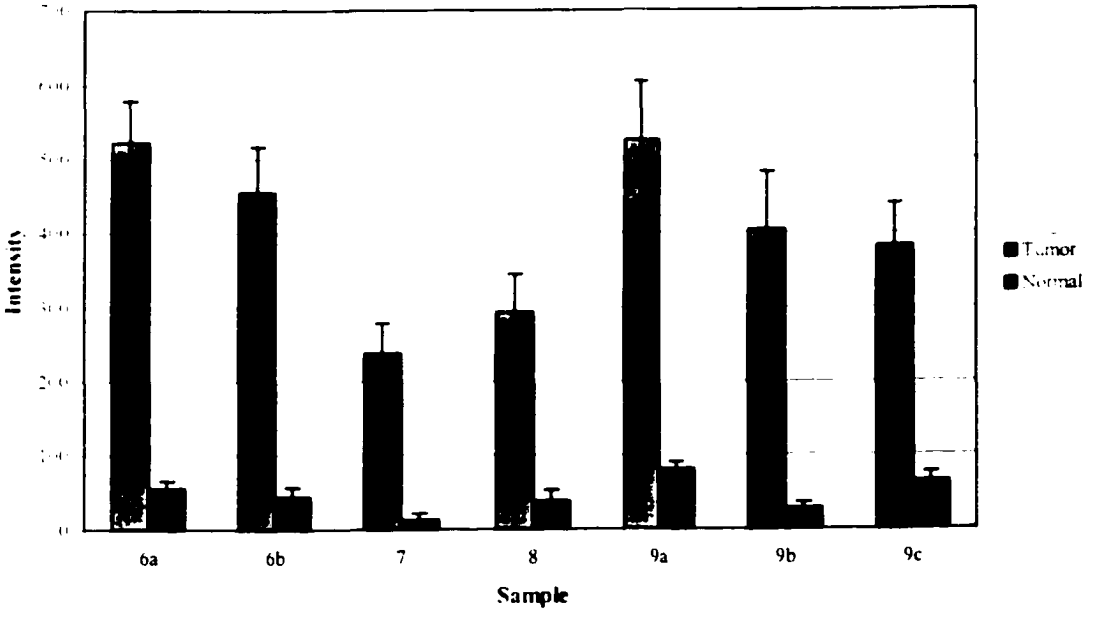

Figure 16. Relative h-ALA-induced fluorescence in biopsy tumors. Samples 6, 7, 8, and 9 were obtained four hours after h-ALA administration.

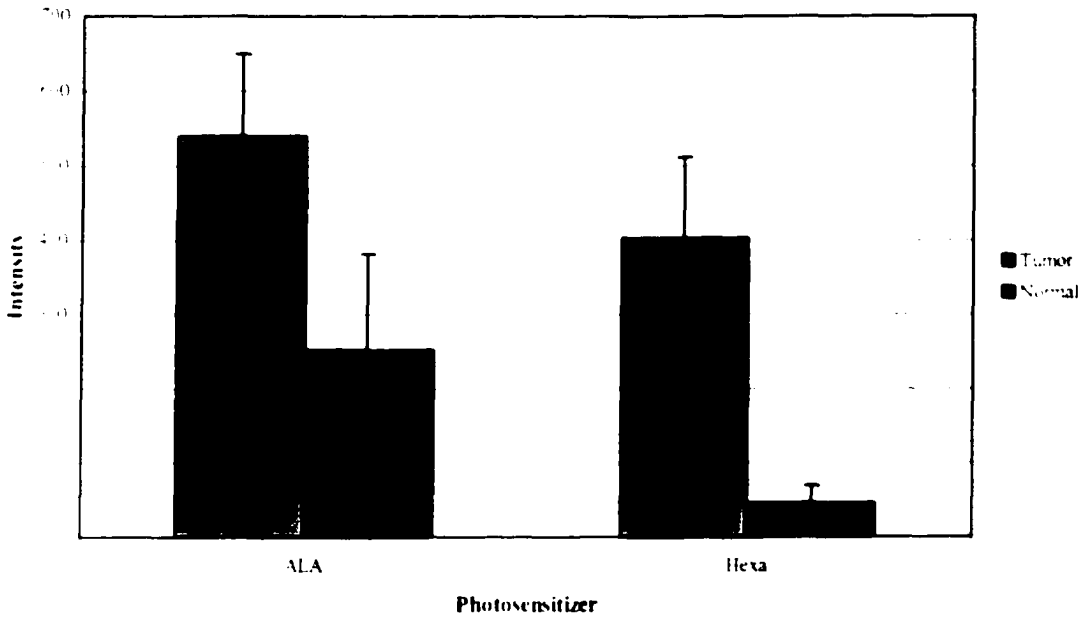

Figure 17. Average relative fluorescence in biopsy tumors. The ALA averages were obtained from Samples 5a, 5b, and 5c (Figure 15). The h-ALA averages were obtained from Samples 6a, 6b, 7, 8, 9a, 9b, 9c (Figure 16).

of PpIX in normal brain tissue, and the resultant high localization ratio,make the h-ALA a promising candidate for investigative brain tumor PDT.

Due to the limited number of adequately developed tumors, the study of photosensitizer distribution in the rat brain following systemic administration was unsuccessful. The vast majority of clinical PDT treatments currently involve the systemic (oral) administration of ALA, with the exception of BCC and squamous cell carcinoma (SCC) treatments in which ALA is administered topically. When considering systemic administration of ALA and its esters, the dose-limiting factor relates primarily to liver toxicity (see Section 1.1.4). The most widely accepted upper limit for systemic administration of ALA is 60 mg kg^{-1} body weight. Relatively little information is known

regarding the uptake of h-ALA following systemic administration. However, h-ALA is more toxic than ALA at lower doses (Peng – unpublished)[*].

While the uniqueness of the biopsy tumor model makes it appealing for use in *in vivo* GBM studies, the actual tumor take (number of tumors that developed following spheroid induction) in this study was rather poor. The proposed titration experiment and systemic administration experiments failed altogether because of a 0% tumor take. A total of 60 rats were injected with biopsy-derived spheroids, 10 of which exhibited noticeable tumor growth. The most probable explanation for this 17% tumor take relates to the tumor-inducing capabilities of the biopsies themselves. Successful biopsy tumor induction depends on spheroid implantation technique. It is possible that variation in the depth of canula placement could adversely affect and or preclude tumor development.

[*] Personal Correspondence

CHAPTER 4

CONCLUSIONS

Foundational toxicity data pertaining to the maximum tolerable ALA and h-ALA doses for local administration in the nude Rowett rat was derived. These animals can safely tolerate 99 mM ALA and 66 mM h-ALA when injected directly into the brain. Although it is unlikely that patients will receive a maximum tolerable dose, a maximal dose used for *in vivo* studies permits a greater PpIX production resulting in improved fluorescence quantification.

The bulk of current *in vivo* experimentation with GBM involves cell-line derived tumors that grow as well-circumscribed, membrane-bound masses. Tumor development associated with cell-line experiments inaccurately represents GBM in patients thus limiting the applicability of the research as it relates to the clinical setting. U-87MG cell-line tumors were used in this study to examine ALA and h-ALA uptake and tumor selectivity as a comparison to the biopsy tumor model. Clearly, based on qualitative observation, photosensitizer transport differs between tumor types (outward diffusion to tumor boundary in cell-line tumors). Quantitative analysis indicates a 4.4±2.5:1 tumor-to-normal tissue uptake with a 7.4±3.0:1 border-to-normal tissue fluorescence following ALA injection. Tumor-to-normal tissue uptake ratios of 20±184:1 and 1.4±0.5:1 were observed in cell-line derived tumors following 1- and 6-hour post h-ALA injection,

respectively. The validity of this data is uncertain due to the small sample size investigated (2 animals).

Qualitatively, fluorescence images of biopsy tumors indicate that the animal model accurately represents GBM in humans. Fluorescence intensity is greatest in the tumor's center and tapers with increasing distance from the tumor. Although a relatively small number of samples were available for analysis, quantitative results agree with several other studies. Following ALA administration, the tumor selectivity was roughly twice that of normal tissue (2.4±1.1:1). H-ALA administration resulted in a higher tumor uptake ratio of 7.6±2.0:1. Due to its enhanced selectivity, the use of h-ALA as a PDT photosensitizing agent should be pursued in further experimentation.

Despite a relatively poor tumor take with the biopsy tumor model, the qualitative fluorescence results reflect the unique property of diffuse tumor infiltration that is currently unavailable with other *in vivo* tumor models. As discussed in Chapter 3, tumor induction might be improved by obtaining a larger quantity of biopsy tissue, which would improve the likelihood of the biopsy containing viable cells. Decreasing the amount of time the biopsy tissue remains outside of an incubator (ie. faster patient-to-lab transport and tissue processing) could improve the tumor-inducing capability of the spheroids. The agreement of quantitative results with published values merits further study with ALA and h-ALA in this biopsy tumor model.

CHAPTER 5

FUTURE STUDY

Due to the novelty of h-ALA, relatively little *in vivo* data regarding its uptake has been obtained. To complement the data acquired in these experiments (pertaining to local administration), the biodistribution of h-ALA should be examined in the rat model following systemic administration. Due to complex delivery logistics associated with local photosensitizer administration in brain tumor treatment, systemic (intravenous) administration in patients is preferred. Furthermore, the systemic administration of h-ALA has been reported to cause severe toxicity effects *in vivo* (van den Boogert *et al* 1998). Systemic h-ALA administration could result in liver and kidney abnormalities that could be of negative consequence to the patient. The potential for patient toxicity provides rationale for further exploration of systemic toxicity effects in the animal model. If a high degree of h-ALA tumor selectivity were achieved after systemic administration, it would be more clinically appealing for PDT than ALA.

To further examine h-ALA biodistribution, the effect of varying photosensitizer concentrations on the production of PpIX should be determined by means of a titration experiment. Although the maximum tolerable photosensitizer dose was administered in this study (to optimize PpIX fluorescence), it would be beneficial to determine if tumor selectivity is jeopardized with decreasing dose and the extent of diminished PpIX production. Clinically, patients are unlikely to receive the maximum tolerable dose (for

toxicity reasons). As a result, the effect of decreasing photosensitizer dose must be understood. Based on the superior h-ALA tumor selectivity observed after one hour of incubation (Sample 3, Figure 8), further study of h-ALA biokinetics is also necessary. Quantifying PpIX production at varying time points would establish the optimal treatment time.

The final process of *in vivo* photosensitizer investigations would involve PDT treatment itself. To determine the effect of improved h-ALA localization, intra-operative PDT would be performed on tumor-bearing rats. Following a waiting period, the animals would be sacrificed and post-treatment tumor size would be measured. Smaller tumor sizes would indicate superior treatment (reflecting superior photosensitizer uptake). *In vivo* studies of this nature are difficult to perform; several logistical barriers must be overcome. Due to the relative size and depth of tumors, and the small burr hole diameter, it would be very difficult to deliver the light dose to the entire tumor. This problem could be overcome by increasing the size of the burr hole but rodents typically develop post-surgical infection with large-scale skull removal. Treatments would likely be performed prior to mature tumor development to permit irradiation of the entire tumor. Unfortunately, short of using magnetic resonance imaging to detect the tumor, there would be no method to determine the extent of tumor development. Additionally, the extent of normal tissue damage following PDT could be examined by using a cell proliferation type assay (such as Ki67).

The potential benefit of PDT in the treatment of aggressive brain tumors warrants further pre-clinical study. Current clinical research in the field of neurosurgery has aimed at developing local photosensitizer delivery systems for PDT. A modified balloon

catheter has been studied as a laser light delivery system that would be employed following GBM resection (Hirschberg *et al* 1999, Madsen *et al* 2001). At present, ALA has been proposed as the photosensitizer for clinical trials because of its tumor selectivity following systemic (oral) administration. For h-ALA to be used in conjunction with the proposed balloon catheter (assuming tumor uptake following local administration only) the catheter must be modified to deliver photosensitizer. It has been suggested that a thin, permeable membrane surrounding the balloon be created to allow diffusion of h-ALA into the resection cavity. However, pre-clinical studies of tumor uptake following systemic h-ALA administration should be performed prior to modifying the catheter mechanism. If h-ALA demonstrates sufficient localization in tumor tissue following systemic administration, several logistical elements regarding its clinical use would be solved.

The role of the MBR in ALA-induced photodamage is currently being studied. The mitochondrial permeability transition (PT) pore regulates mitochondria membrane permeability. PT may be inhibited or induced by the interaction of anti-apoptotic or pro-apoptotic factors with the PT pore. Current research aims at using agents that target the PT pore in conjunction with ALA-mediated PDT to overcome apoptosis-inhibiting factors such as Bcl-2 proteins. This form of therapy would enhance the effect of PDT by inducing apoptosis in tumor cells.

REFERENCES

Ackroyd R, Brown N, Vernon D, Roberts D, Stephenson T, Marcus S, Stoddard C, Reed M. 1999. 5-Aminolevulinic acid photosensitization of dysplastic Barrett's esophagus: a pharmacokinetic study. Photochem Photobiol. 70:656-62.

Agarwal ML, Clay ME, Harvey EJ, Evans HH, Antunez AR, Oleinick NL. 1991. Photodynamic therapy induces rapid cell death by apoptosis in L5178Y mouse lymphoma cells. Cancer Res. 51:5993-5996.

Anderson AP. 1978. Postoperative irradiation for glioblastomas. Results of a randomized series. Acta Radiol 17:474-484.

Bedwell J, MacRobert AJ, Phillips D, Bown SG. 1992. Fluorescence distribution and photodynamic effect of ALA-induced PPIX in the DMH rat colonic tumor model. Br J Cancer. 65:818-824.

Black PM. 1991. Brain tumors, part 1. N Engl J Medicine. 324:1471-1476.

Bunke A, Zerbe O, Schmid H, Burmeister G, Merkle HP, Gander B. 2000. Degradation mechanism and stability of 5-aminolevulinic acid. J Pharm Sci. 89:1335-1341.

Chang S-C, MacRobert AJ, Bown SG. 1996. Biodistribtion of protopophyrin IX in rat urinary bladder after intravesical instillation of 5-aminolevulinic acid. J Urology 155:1744-1748.

Dougherty TJ, Gomer CJ, Henderson BW, Jori G, Kessel D, Korbelik M, Joan J, Peng Q. 1998. Photodynamic therapy. J Natl Cancer Inst. 90:889-905.

Egger NG, Motamedi M, Pow-Sang M, Orihuela E, Anderson KA. 1996. Accumulation of porphyrins in plasma and tissues of dogs after aminolevulinic acid administration. Implication for photodynamic therapy. Pharmacology. 52:362-370.

Emami B, Lyman J, Brown A, Coia L, Goitein M, Munzenrider JE, Shank B, Solin LG, Wessom M. 1992. Tolerance of normal tissue to therapeutic irradiation. Intl J Rad Oncol Biol Phys. 21:109-122.

Engebraaten O, Hjortland GO, Hisrchberg H, Fodstad O. 1999. Growth of precultured human glioma specimens in nude rat brain. J Neurosurg. 90:125-132.

Fine HA. 1994. The basis for current treatment recommendations for malignant gliomas. J Neurooncol. 20:111-120.

Fisher DE. 1994. Apoptosis in cancer therapy: crossing the threshold. Cell. 78:539-542.

Fukuda H, Casas A, Chueke F, Paredes S, Batlle AMC. 1993. Photodymaic action of endogenously synthesized porphryins from aminolevulinic acid, using a new model for assaying the effectiveness of tumoral cell killing. Intl J Biochem. 25:1395-1398.

Gossner L, May A, Sroka R, Stolte M, Ell C. 1999. Photodynamic destruction of high grade dysplasia and early carcinoma of the esophagus after the oral administration of 5-aminolevulinic acid. Cancer. 86:1921-1928.

Groothuis DR. 2000. The blood-brain and blood-tumor barriers: a review of strategies for increasing drug delivery. Neurooncology. 2:45-59.

Hasan T and Parrish JA. 1997. Photodynamic therapy of cancer. In: Cancer Medicine, 4th ed. (Holland JF, Frei EI, Bast RCJ, Kufe DW, Morton DL, Weichselbaum RR, Eds.). p. 739-750. Baltimore: Williams & Wilkins.

Hasegowa H, Ushio Y, Hayakawa T, Yamada K, Mogami H. 1983. Changes of the blood-brain barrier in experimental metastatic brain tumor. J Neurosurg. 59:304-310.

He J and Oleinick NL. 1995. Cell death mechanisms vary with photodynamic therapy dose and photosensitizer. SPIE. 2371:92-96.

He XY, Sikes R, Thomsen S, Chung LWK, Jacques SL. 1994. Photodynamic Therapy with Photofrin II induces programmed cell death in carcinoma cell lines. Photochem Photobiol. 59:468-473.

Hebeda KM, Saarnak AE, Olivo M, Sterenborg HJCM, Wolbers JG. 1998. 5-Aminolevulinic acid induced endogenous porphyrin fluorescence in 9L and C6 brain tumours and in the normal rat brain. Acta Neurochir (Wien). 140:503-513.

Henderson BW, Vaughan L, Bellnier DA, van Leengoed H, Johnson PG, Oseroff AR. 1995. Photosensitization of murine tumor, vasculature and skin by using 5-aminolevulinic acid-induced porphyrin. Photochem Photobiol. 62:780-789.

Henderson BW and Dougherty TJ. 1992. How does photodynamic therapy work? Photochem Photobiol. 55:145-157.

Hinnen P, Rooij FWM, Terlouw EM, Edixhoven A, van Dekken H, van Hillegersberg R, Tilanus HW, Wilson JHP, Siersema PD. 2000. Porphyrin biosynthesis in human

Barrett's oesophagus and adenocarcinoma after ingestion of 5-aminolevulinic acid. Br J Cancer. 83:539-543.

Hischberg H, Madsen S, Lote K, Pham T, Tromberg B. 1999. An indwelling brachytherapy balloon catheter: potential use as an intracranial light applicator for photodynamic therapy. J Neurooncol. 44:15-21.

Hirschberg H, Sun CH, Tromberg BJ, Madsen SJ. 2002. ALA- and ALA-ester-mediated photodynamic therapy of human glioma spheroids. J Neurooncol 57:1-7.

Hua Z, Gibson SL, Foster TH, Hilf R. 1995. Effectiveness of delta-aminolevulinic acid-induced protoporphyrin as a photosensitizer for photodynamic therapy *in vivo*. Cancer Res. 55:1723-1731.

Kerr JFR, Wyllie AH, Currie AR. 1972. Apoptosis: a basic biologic phenomenon with wide-ranging implications in tissue kinetics. Br J Cancer. 26:239-257.

Kessel D, Luo Y, Deng Y, Chang CK. 1997. The role of sub-cellular localization in initiation of apoptosis by photodynamic therapy. Photochem Photobiol. 65:422-426.

Kessel D and Luo Y. 1998. Mitochondrial photodamage and PDT-induced apoptosis. J. Photochem Photobiol B. 42:89-95.

Kessel D, Luo Y, Chang CK, Henderson BW, Woodburn K. 1998. Modes of Cytotoxicity Associated with Photodynamic Therapy. SPIE. 2972:103-109.

Kloek J, Akkermans W, Beijersbergen van Henegouwen GM. 1998. Derivatives of 5-aminolevulinic acid for photodynamic therapy: enzymatic conversion into protoporphryin IX. Photochem Photobiol. 67:150-154.

Kloek J and van Henegouwen B. 1996. Prodrugs of 5-aminolevulinic acid for photodynamic therapy. Photochem Photobiol. 64:994-1000.

Kluck RM, Bossy-Wetzel E, Greene DR, Newmeyer DW. 1997. The release of cytochrome c from mitochondria: a primary site of Bcl-2 regulation of apoptosis. Science. 275:1132-1136.

Krems IJ and Spoerri PE. 1947. The pyrazines. Chem Rev. 40:290-358.

Kristiansen K, Hagen S, Kollevold T, Torvik A, Holme I, Nesbakken R, Hatlevoll R, Lindgren M, Brun A, Lindgren S, Notter G, Andersen AP, Elgen K. 1981. Combined modality therapy of operated astrocytomas grade III and IV. Confirmation of the value of post-operative irradiation and lack of potentiation of bleomycin on survival time: a prospective multicenter trial of the Scandinavian Glioblastoma Study Group. Cancer 47: 649-652.

Lilge L and Wilson BC. 1998. Photodynamic therapy of intracranial tissues: a preclinical comparative study of four different photosensitizers. J Clin Laser Med Surg. 16:81-91.

Liu X, Kim J, Yang J, Jemmerson R, Wang X. 1996. Induction of apoptotic program in cell-free extracts: requirement for dATP and cytochrome *c*. Cell. 86:147-157.

Loh CS, MacRobert AL, Bedwell J, Regula J, Krasner N, Brown SG. 1993. Oral versus intravenous administration of 5-aminolaevulinic acid for photodynamic therapy. Br J Cancer. 68:41-51.

Luo Y and Kessel D. 1997. Initiation of apoptosis versus necrosis by photodynamic therapy with chloroaluminum phthalocyanine. Photochem Photobiol. 66:479-483.

Luo Y, Chang CK, Kessel D. 1996. Rapid initiation of apoptosis by photodynamic therapy. Photochem Photobiol. 63:528-534.

Madsen SJ, Sun CH, Tromberg BJ, Hirschberg H. 2001. Development of a novel indwelling balloon applicator for optimizing light delivery in photodynamic therapy. Lasers Surg Med. 29:406-412.

McGillion FB, Thompson GG, Moore MR, Goldberg A. 1974. The passage of 5-aminolevulinic acid across the blood brain barrier of the rat: effect of ethanol. Biochem Pharmacol. 23:472-474.

McGillion FB, Thompson GG, Goldberg A. 1975. Tissue uptake of 5-aminolevulinic acid. Biochem Pharmacol. 24:299-301.

Moan J and Berg K. 1992. Photochemotherapy of cancer: Experimental research. Photochem Photobiol. 55:931-948.

Moan J and Berg K. 1991. The photodegradation of porphyrins in cells can be used to estimate the lifetime of singlet oxygen. Photochem Photobiol. 53:549-553.

Moore JV, West CM, Whitehurst C. 1997. The biology of photodynamic therapy. Phys Med Biol. 42:913-935.

Muller PJ and Wilson BC. 1985. Photodynamic therapy: cavitary photoillumination of malignant cerebral tumors using a laser coupled inflatable balloon. Can J Neurol Sci. 12:371-373.

Muller PJ and Wilson BC. 1996. Photodynamic therapy for malignant newly diagnosed supratentorial gliomas. J Clin Laser Med Surg. 14:263-270.

Noodt B, Berg K, Stokke T, Peng Q, Nesland JM. 1996. Apoptosis and necrosis induced with light and 5-aminolevulinic acid-derived protoporphyrin IX. Br J Cancer. 74:22-29.

Novo M, Huttmann G, Diddens H. 1996. Chemical instability of 5-aminolevulinic acid used in the fluorescence diagnosis of bladder tumours. J Photochem Photobiol B. 34:143-148.

Ochsner M. 1997. Photophysical and photobiological processes in the photodynamic therapy of tumors. J Photochem Photobiol B. 39:1-18.

Oleinick NL and Evans HH. 1998. The photobiology of photodynamic therapy: cellular targets and mechanisms. Radiat Res. 150(5 Suppl):S146-156.

Olivo MC, Kweicien JM, Wilson BC. [Fluorescence distribution of ALA-induced PpIX in rabbit brain and intracranial tumor using confocal fluorescence microscopy.]

Pastorino JG, Simbula G, Gilfor E, Hoek JB, Farber JL. 1994. Protoporphyrin IX, and endogenous ligand of the peripheral benzodiapepine receptor, potentiates induction of the mitochondrial permeability transition and the killing of cultured hepatocytes by rotenone. J Biol Chem. 269:31041-31046.

Patterson MS, Madsen SJ, Wilson BC. 1990. Experimental tests of the feasibility of singlet oxygen luminescence monitoring in vivo during photodynamic therapy. J Photochem Photobiol B. 5:69-84.

Peng Q, Soler AM, Warloe T, Nesland JM, Geircksky KE. 2001. Selective distribution of porphryins in skin thick basal cell carcinoma after topical application of methyl 5-aminolevuliniate. J Photochem Photobiol B. 62:140-145.

Peng Q, Berg K, Moan J, Kongshaug M, Nesland JM. 1997. 5-Aminolevulinic acid-based photodynamic therapy: principles and experimental research. Photochem Photobiol. 65:235-251.

Peng Q, Moan J, Warloe T, Nesland JM, Rimington C. 1992. Distribution and photosensitizing efficiency of porphyrins induced by application of exogenous 5-aminolevulinic acid in mice bearing mammary carcinoma. Intl J Cancer. 52:433-443.

Popovic EA, Kaye AH, Hill JS. 1995. Photodynamic therapy of brain tumors. Sem Surg Oncol. 11:335-345.

Stummer W, Novotny A, Stepp H, Goetz C, Bise K, Reulen HJ. 2000. Fluorescence-guided resection of glioblastoma multiforme by using 5-aminolevulinic acid-induced porphyrins: a prospective study in 52 consecutive patients. J Neurosurg. 93:1003-1013.

Stummer W and Baumgartner R. 2000. Fluorescence-guided resection of malignant gliomas utilising 5-ALA-induced porphyrins. Photodynamics. 3:6-7.

Stummer W, Stepp H, Möller G, Ehrhardt A, Leonhard M, Reulen HJ. 1998a. Technical principles for protoporphyrin-IX-fluorescence guided microsurgical resection of malignant glioma tissue. Acta Neurochir (Wien). 140: 995-1000.

Stummer W, Stocker S, Wagner S, Stepp H, Fritsch C, Goetz C, Goetz AE, Kiefmann R, Reulen HJ. 1998b. Intraoperative detection of malignant gliomas by 5-aminolevulinic acid-induced porphyrin fluorescence. Neurosurgery. 42:518-526.

Stummer W, Stocker S, Novotny A, Heimann A, Sauer O, Kempski O, Plesnila N, Wietzorrek J, Reulen HJ. 1998c. In vitro and in vivo porphyrin accumulation by C6 glioma cells after exposure to 5-aminolevulinic acid. Journal of Photochem Photobiol B. 45:160-169.

Terr L and Weiner LP. 1983. An autoradiographic study of 5-aminolevulinic acid uptake by mouse brain. Exp Neurol. 79:564-568.

Tope WD, Ross EV, Kollias N, Martin A, Gillies R, Anderson RR. 1998. Protoporphyrin IX fluorescence induced basal cell carcinoma by oral aminolevulinic acid. Photochem Photobiol. 67:249-255.

Uehlinger P, Zellweger M, Wagnieres G, Juillerat-Jeanneret L, van den Bergh H, Lange N. 2000. 5-Aminolevulinic acid and its derivatives: physical chemical properties and protoporphyrin IX formation in cultured cells. J Photochem Photobiol B. 54:72-80.

van den Boogert J, van Hillegersberg R, de Rooij FW, de Bruin RW, Edixhoven-Bosdijk A, Houtsmuller AB, Siersema PD, Wilson JH, Tilanus HW. 1998. 5-Aminolaevulinic acid-induced protoporphyrin IX accumulation in tissues: pharmacokinetics after oral or intravenous administration. J Photochem Photobiol B. 44:29-38.

Vaux DL and Strassner A. 1996. The molecular biology of apoptosis. Proc Natl Acad Sci USA. 93:2239-2244.

Verma A, Hirsch DJ, Galtt CE, Ronnett GV, Snyder SH. 1993. Carbon monoxide, a putative neural messenger. Science. 259:381-384.

Walker MD, Alexander E Jr, Hunt WE, MacCarty CS, Mahaley MS Jr, Mealey J Jr, Norrell HA, Owens G, Ransohoff J, Wilson CB, Gehan EA, Strike TA. 1978. Evaluation of BCNU and/or radiotherapy in the treatment of anaplastic gliomas. J Neurosurg. 49:333-343.

Walker MD, Green SB, Byar DP, Alexander E Jr, Batzdorf U, Brooks WH, Hunt WE, MacCarty CS, Mahaley MS Jr, Mealey J Jr, Owens G, Ransohoff J 2nd, Robertson JT, Shapiro WR, Smith KR Jr, Wilson CB, Strike TA. 1980. Randomized comparison of radiotherapy and nitrosureas for treatment of malignant glioma after surgery. N Engl J Med. 303:1323-1329.

Webber J, Luo Y, Crilly R, Fromm D, Kessel D. 1996. An apoptotic response to photodynamic therapy with endogenous protoporphyrin in vivo. J Photochem Photobiol B. 35:209-211.

Webber J, Kessel D, Fromm D. 1997. Side effects and photosensitation of human tissues after aminolevulinic acid. J Surg Res. 68:31-37.

Weishaupt KR, Gomer CJ, Dougherty TJ. 1976. Identification of singlet oxygen as the cytotoxic agent in photoinactivation of a murine tumor. Cancer Res. 36:2326-2329.

Williams GT. 1991. Programmed cell death: apoptosis and oncogenesis. Cell. 65:1097-1098.

Wyllie AH. 1985. The biology of cell death in tumors. Anticancer Res. 5:131-136, 1985.

Xiao Z, Miller GG, McCallum TJ, Brown KM, Lown JW, Tulip J, Moore RB. 1998. Biodistribution of Photofrin II and 5-aminolevulinic acid-induced protoporphyrin IX in normal rat bladder and bladder tumor models: implications for photodynamic therapy. Photochem Photobiol. 67:573-583.

Yamada K, Ushio Y, Hayakawa T, Kato A, Yamada N, Mogami H. 1982. Quantitative autoradiographic measurements of blood-brain barrier permeability in the rat glioma model. J Neurosurg. 57:394-398.

Yang J, Bhalla K, Kim CN, Ibrado AM, Peng TI, Jones DP, Wang X. 1997. Prevention of apoptosis by Bcl-2: release of cytochrome c from mitochondria blocked. Science. 275:1129-1132.

Zaidi SIA, Oleinick NL, Zaim MT, Mukhtar H. 1993. Apoptosis during photodynamic therapy-induced ablation of RIF-1 tumors in C3H mice: electron microscopic, hisopathologic and biochemical evidence. Photochem Photobiol. 58:771-776.